Robust Convex Approximation Methods for TDOA-Based Localization under NLOS Conditions

Gang Wang, *Member, IEEE,* Anthony Man-Cho So, *Member, IEEE,* and Youming Li

***Abstract*—In this paper, we develop a novel robust optimization approach to source localization using time-difference-of-arrival (TDOA) measurements that are collected under non-line-of-sight (NLOS) conditions. A key feature of our approach is that it does not require knowledge of the distribution or statistics of the NLOS errors, which are often difficult to obtain in practice. Instead, it only assumes that the NLOS errors have bounded supports. Based on this assumption, we formulate the TDOA-based source localization problem as a robust least squares (RLS) problem, in which a location estimate that is robust against the NLOS errors is sought. Since the RLS problem is non-convex, we propose two efficiently implementable convex relaxation-based approximation methods to tackle it. We then conduct a thorough theoretical analysis of the approximation quality and computational complexity of these two methods. In particular, we establish conditions under which they will yield a unique localization of the source. Simulation results on both synthetic and real data show that the performance of our approach under various NLOS settings is very stable and is significantly better than that of several existing non-robust approaches.**

***Index Terms*—Robust Localization, Time-Difference of Arrival (TDOA), Non-Line of Sight (NLOS), Convex Relaxation**

I. Introduction

The accurate localization of a signal-emitting source is key to a number of applications, such as emergency service [1] and response [2], mobile computing [3], and target tracking [4]. In a typical scenario, the localization is facilitated by a network of sensors, which collect location metrics of the source. Two commonly used metrics are the source signal's time of arrival (TOA) and time-difference of arrival (TDOA). Assuming the signal propagation speed is fixed and known, the former gives rise to range measurements between the source and the sensors, while the latter to range-difference measurements. These measurements can then be used to estimate the source location. We refer the uninitiated reader to [5], [6] and the references therein for an overview of various localization concepts and techniques.

Naturally, errors in the TOA and TDOA measurements will have an adverse effect on localization accuracy. A predominant type of error arises from the so-called non-line-of-sight (NLOS) condition—i.e., when the direct, or line-of-sight (LOS), paths between the source and the sensors are blocked, thereby resulting in additional, variable propagation delay of the source signal. NLOS errors are common in indoor and urban settings, and if not treated properly, they can severely degrade the quality of the estimated location. Therefore, the problem of NLOS identification and mitigation has attracted much attention in recent years. One popular approach is to utilize certain knowledge of the NLOS errors (such as their joint probability distribution, statistics, or physical attributes) and estimate the source location via a maximum-likelihood or penalty function formulation; see, e.g., [7]–[11] and the references therein. Such an approach is effective when the NLOS errors are modeled accurately. However, since the characteristics of the NLOS errors are generally environment and time dependent, it can be costly and tedious to build good models of them. To circumvent this difficulty, researchers have considered approaches that are less reliant on precise knowledge of the NLOS errors. We refer the reader to [7], [12]–[15] and the references therein for some of the latest advances in this direction.

Although there is a vast literature addressing the issue of NLOS identification and mitigation in localization, most of it focuses on TOA-based systems. Given the less stringent synchronization requirements and wide applicability of TDOA-based systems, it is natural to ask whether the techniques developed for TOA-based systems can be applied to TDOA-based ones. As it turns out, the answer is not so straightforward. First, in a TDOA measurement, the error caused by the NLOS condition is the difference of the NLOS errors incurred at two different sensors. As such, its distribution is different from that of the NLOS error at each sensor and does not admit a simple characterization in general. This not only complicates the implementation of maximum-likehood estimators (cf. [9], [16]) but also degrades the performance of TDOA-based localization methods that do not take the effects of NLOS errors into account; see Section V. Second, by exploiting the fact that the NLOS error in a TOA measurement is always non-negative and is typically much larger than the measurement noise, one can limit the region in which the source lies, thereby improving

This research is supported by the National Natural Science Foundation of China under Grant 61201099 and 61571249, the Open Foundation of the State Key Laboratory of Integrated Services Networks, Xidian University, under Grant ISN16-05, the Zhejiang Open Foundation of the Most Important Subjects of Information and Communication Engineering under Grant xkx11401, the Research Project of Zhejiang Provincial Department of Education under Grant Y201224625, the K. C. Wong Magna Fund in Ningbo University, and the Hong Kong Research Grants Council (RGC) General Research Fund (GRF) Project CUHK 416413.

G. Wang and Y. Li are with the Faculty of Electrical Engineering and Computer Science, Ningbo University, Ningbo 315211, China. G. Wang is also with the State Key Laboratory of Integrated Services Networks, Xidian University, Xi'an 710071, China (e-mail: wanggang@nbu.edu.cn, liyouming@nbu.edu.cn). This work was done during the first author's visit at The Chinese University of Hong Kong.

A. M.-C. So is with the Department of Systems Engineering and Engineering Management, and, by courtesy, the CUHK-BGI Innovation Institute of Trans-omics, The Chinese University of Hong Kong, Shatin, N. T., Hong Kong (email: manchoso@se.cuhk.edu.hk).

the localization accuracy [14], [17]–[19]. On the other hand, due to potential cancellations of the NLOS errors at different sensors, the error caused by the NLOS condition in a TDOA measurement can be negative and/or small in magnitude. Thus, the above strategy does not work. Nevertheless, the analysis in [20] shows that when many of the source-sensor paths are NLOS, one can achieve better localization performance with TDOA measurements than with TOA measurements. This conforms with the intuition that smaller errors should produce more accurate estimates. Unfortunately, it is not clear if the theoretical localization performance established in [20] can be realized by an efficient algorithm.

From the above discussion, we see that the algorithmic aspects of TDOA-based localization under NLOS conditions are still under-explored and deserve further investigation. In this paper, we take a step in this direction by developing a robust optimization approach to NLOS mitigation in TDOA-based localization. Our approach does not need to distinguish between LOS and NLOS measurements, nor does it require *a priori* knowledge of the distribution or statistics of the NLOS errors. All it assumes is that the magnitudes of the NLOS errors are upper bounded by some given constants. The rationale behind this approach is that it is often easier to estimate the support of the NLOS error distribution than the distribution itself. In addition, such an approach is less sensitive to misspecifications of the error distribution model.

Based on the upper bounds on the magnitudes of the NLOS errors, we formulate the source localization problem as a robust least squares (RLS) problem. The RLS problem is non-convex and generally intractable. Worse yet, it is not immediately amenable to convex relaxation techniques. To circumvent these difficulties, we first construct an auxiliary problem that approximates the original RLS problem. Although the auxiliary problem is still non-convex, it can be tackled by convex relaxation techniques. Moreover, we can rigorously identify the conditions under which the auxiliary problem is equivalent to the RLS problem. These conditions have a simple interpretation in the context of NLOS TDOA-based localization and offer much insight into the efficacy of our proposed approach; see Section IV-A. Then, we propose a second-order cone relaxation (SOCR) and a natural semidefinite relaxation (SDR) of the auxiliary problem, both of which are polynomial-time solvable [21, Lecture 6] and can be easily implemented using off-the-shelf softwares (e.g., `CVX` [22]). Curiously, it can be shown that the natural SDR is weaker than the SOCR, which is contrary to the widely-held belief that second-order cone relaxations are weaker than semidefinite relaxations (compare, e.g., [23]–[25]). Nevertheless, by adding a set of valid inequalities to the SDR, we obtain a refined SDR that is provably tighter than the SOCR and is also efficiently solvable. As our final theoretical contribution, we establish sufficient conditions for the SOCR and the refined SDR to yield a unique localization of the source. Interestingly, our simulation results show that the sufficient conditions are satisfied under a wide variety of settings; see Section V.

It should be emphasized that our approach, which is based on the *robust optimization* methodology, is very different from the *robust statistics*-based approach that has been extensively investigated in the literature (see, e.g., [11], [15], [26] and the references therein). The latter is mainly developed for TOA-based localization, where the NLOS measurements can be treated as outliers and the aggregate measurement error is modeled as a random variable with simple mixture distribution. By estimating certain statistical parameters of the error distribution, one obtains source location estimates that are statistically efficient and not unduly affected by outliers. However, it is non-trivial to develop an analogous approach for TDOA-based localization, as the error distribution typically has much more complex properties and cannot be captured by a simple model. By contrast, the former only assumes that the NLOS errors have bounded magnitudes and aims at producing source location estimates that have high accuracy regardless of the realization of the NLOS errors. As such, the robust optimization-based approach does not require the specification of any error distribution model and hence can be easily applied to TDOA-based localization.

We note that the robust optimization methodology has been used before to deal with uncertainties in the sensors' positions [27] and in the NLOS errors in TOA-based localization [14]. Our work is closer in spirit to the latter, though the development is different. Specifically, the formulation in [14] essentially assumes that the vector of NLOS errors lies in a ball. This, together with the $\mathcal{S}$-lemma [21], immediately yields a tractable reformulation of the corresponding robust problem. However, the ball constraint imposes a non-trivial correlation structure among the NLOS errors, which is difficult to justify. By contrast, our formulation assumes that the vector of NLOS errors lies in a box and hence does not have the said issue. Moreover, as the $\mathcal{S}$-lemma no longer applies in our setting, we need to develop new analytical tools to reformulate the resulting robust problem into a tractable form. Lastly, we conduct a thorough analysis of our formulations, which yields new theoretical results for TDOA-based localization.

The remainder of this paper is organized as follows. In Section II, we describe the TDOA measurement model under NLOS conditions, based on which we give an RLS formulation of the source localization problem. Next, in Section III, we introduce the auxiliary problem that approximates the RLS problem and present the SOCR and SDR methods for tackling the auxiliary problem. In Section IV, we identify the conditions under which the auxiliary problem is equivalent to the RLS problem. We also analyze the relative tightness, complexity, and unique localizability of the proposed convex relaxations of the auxiliary problem. Then, in Section V, we illustrate our proposed methods via numerical simulations on both synthetic and real data. Finally, we close with some concluding remarks in Section VI.

The following notation will be adopted throughout the article. Bold face lower case letters and bold face upper case letters denote vectors and matrices, respectively. a_i denotes the ith element of the vector $\boldsymbol{a}$ and $A_{i,j}$ denotes the (i,j)th element of the matrix $\boldsymbol{A}$. $\mathbf{0}_{k\times l}$ denotes the $k\times l$ all-zero matrix; $\mathbf{1}_k$ and $\boldsymbol{I}_k$ denote the $k\times 1$ all-one column vector and the $k\times k$ identity matrix, respectively. Given numbers $a_1,\ldots,a_l$, $\mathrm{Diag}(a_1,\ldots,a_l)$ denotes the $l\times l$ diagonal matrix with $a_1,\ldots,a_l$ on the diagonal. $\mathrm{tr}(\boldsymbol{A})$ and $\mathrm{rank}(\boldsymbol{A})$ stand for

the trace and rank of $\boldsymbol{A}$, respectively. $\mathbb{R}^n$ and $\mathbb{S}^n$ denote the sets of n-dimensional real vectors and $n \times n$ real symmetric matrices, respectively. For $\boldsymbol{A}, \boldsymbol{B} \in \mathbb{S}^n$, $\boldsymbol{A} \succeq \boldsymbol{B}$ means that $\boldsymbol{A} - \boldsymbol{B}$ is positive semidefinite.

II. Problem Formulation

Consider the problem of using TDOA measurements from a wireless sensor network with $N+1$ sensors to localize one unknown source, where the signal propagation paths between the source and the sensors are possibly NLOS. By designating the zeroth sensor as the reference sensor, we assume that the TDOA measurement model takes the form

$$t_i = \frac{1}{c}(\|\boldsymbol{x} - \boldsymbol{s}_i\| - \|\boldsymbol{x} - \boldsymbol{s}_0\| + n_i + e_i) \quad \text{for } i = 1, \ldots, N, \tag{1}$$

where $\boldsymbol{x} \in \mathbb{R}^d$ is the source location that needs to be estimated; $\boldsymbol{s}_i \in \mathbb{R}^d$ (for $i = 0, 1, \ldots, N$) is the location of the ith sensor, which is assumed to be known; c is the signal propagation speed, which is also assumed to be known; $\frac{1}{c}n_i$ and $\frac{1}{c}e_i$ (for $i = 1, \ldots, N$) are the measurement noise and NLOS error at the ith sensor, respectively; d is the dimension in which the source and sensors reside. Naturally, the case where $d \leq 3$ is of most practical interest, though it should be noted that our subsequent development applies to any $d \geq 1$.

By multiplying c on both sides of (1), we obtain the range-difference measurements

$$d_i = \|\boldsymbol{x} - \boldsymbol{s}_i\| - \|\boldsymbol{x} - \boldsymbol{s}_0\| + n_i + e_i \quad \text{for } i = 1, \ldots, N. \tag{2}$$

To localize the source, a typical approach is to treat the errors n_i, e_i as random variables and formulate an (approximate) maximum-likelihood estimation problem; see, e.g., [9], [16]. However, the efficacy of this approach depends on how well the error distributions can be modeled. While it has been widely accepted that the measurement noise n_i can be modeled using the Gaussian distribution (see, e.g., [5], [14], [16]–[20]), the environment- and time-varying nature of NLOS errors makes it difficult to build an accurate model of the distribution of e_i. Even if one has such a model, its complexity can render the resulting maximum-likelihood problem intractable. As an alternative, we propose a robust optimization approach to source localization using the TDOA measurement model (1). To begin, let us state our assumptions on the measurement noise n_i and NLOS error e_i, where $i = 1, \ldots, N$:

(a) The magnitude of the measurement noise n_i is small compared with the range between the source and the reference sensor; i.e., $|n_i| \ll \|\boldsymbol{x} - \boldsymbol{s}_0\|$.

(b) The magnitude of the NLOS error e_i is bounded by some given constant $\rho_i \geq 0$; i.e., $|e_i| \leq \rho_i$.

Assumption (a) is standard in the localization literature (see, e.g., [28]) and can be satisfied using suitable hardware (see, e.g., [29]). Assumption (b) is motivated by the fact that it is easier to estimate the support of a distribution than the distribution itself [30]. In practice, the upper bounds ρ_i (for $i = 1, \ldots, N$) can be estimated in the calibration stage using some training data. In the sequel, we shall make no other assumptions on the distributions of n_i and e_i besides (a) and (b).

Now, the range-difference measurements (2) are equivalent to

$$d_i - e_i - \|\boldsymbol{x} - \boldsymbol{s}_i\| = -\|\boldsymbol{x} - \boldsymbol{s}_0\| + n_i \quad \text{for } i = 1, \ldots, N. \tag{3}$$

Upon squaring both sides of (3) and invoking Assumption (a), we have

$$\begin{aligned}(d_i - e_i)^2 - 2(d_i - e_i)\|\boldsymbol{x} - \boldsymbol{s}_i\| - 2\boldsymbol{s}_i^T\boldsymbol{x} + 2\boldsymbol{s}_0^T\boldsymbol{x} \\ + \|\boldsymbol{s}_i\|^2 - \|\boldsymbol{s}_0\|^2 \approx -2\|\boldsymbol{x} - \boldsymbol{s}_0\|n_i\end{aligned}$$

for $i = 1, \ldots, N$, or equivalently,

$$\begin{aligned}(\boldsymbol{a}_i + \Delta\boldsymbol{a}_i)^T\boldsymbol{y} - (b_i + \Delta b_i) \approx -2\|\boldsymbol{x} - \boldsymbol{s}_0\|n_i \\ \text{for } i = 1, \ldots, N,\end{aligned} \tag{4}$$

where $\boldsymbol{y} = \left[\boldsymbol{x}^T, \|\boldsymbol{x} - \boldsymbol{s}_1\|, \ldots, \|\boldsymbol{x} - \boldsymbol{s}_N\|\right]^T \in \mathbb{R}^{d+N}$,

$$\boldsymbol{a}_i = \left[2(\boldsymbol{s}_0 - \boldsymbol{s}_i)^T, \boldsymbol{0}_{1\times(i-1)}, -2d_i, \boldsymbol{0}_{1\times(N-i)}\right]^T \in \mathbb{R}^{d+N}, \tag{5}$$

$$\begin{aligned}\Delta\boldsymbol{a}_i &= \left[\boldsymbol{0}_{1\times d}, \boldsymbol{0}_{1\times(i-1)}, 2e_i, \boldsymbol{0}_{1\times(N-i)}\right]^T \in \mathbb{R}^{d+N}, \\ b_i &= \|\boldsymbol{s}_0\|^2 - \|\boldsymbol{s}_i\|^2 - d_i^2, \quad \Delta b_i = -e_i^2 + 2d_ie_i.\end{aligned} \tag{6}$$

Based on (4) and Assumptions (a) and (b), we formulate the source localization problem as the following *worst-case* robust least squares (RLS) problem:

$$\begin{aligned}\min_{\boldsymbol{y}=[\boldsymbol{x}^T,\boldsymbol{r}^T]^T\in\mathbb{R}^{d+N}} \quad & \max_{-\boldsymbol{\rho}\leq\boldsymbol{e}\leq\boldsymbol{\rho}} \sum_{i=1}^N \left|\boldsymbol{a}_i^T\boldsymbol{y} - b_i + \Delta\boldsymbol{a}_i^T\boldsymbol{y} - \Delta b_i\right|^2 \\ \text{s.t.} \quad & \|\boldsymbol{x} - \boldsymbol{s}_i\| = r_i \quad \text{for } i = 1, \ldots, N.\end{aligned} \tag{7}$$

Here, we use $\boldsymbol{r} = [r_1, \ldots, r_N]^T$, $\boldsymbol{e} = [e_1, \ldots, e_N]^T$, and $\boldsymbol{\rho} = [\rho_1, \ldots, \rho_N]^T$ to denote the vectors whose ith entries (for $i = 1, \ldots, N$) are the range between the source and the ith sensor, the NLOS error at sensor i, and the upper bound on the magnitude of the NLOS error at sensor i, respectively. Roughly speaking, our goal is to find the source location $\boldsymbol{x}$ such that for $i = 1, \ldots, N$, the deviation of the range difference $\|\boldsymbol{x} - \boldsymbol{s}_i\| - \|\boldsymbol{x} - \boldsymbol{s}_0\|$ from the measured value d_i is small, regardless of the realization of the NLOS error e_i.

III. Convex Approximations of the RLS Problem

To develop efficient methods for tackling the RLS problem (7), we proceed as follows. Observe that for any given $\boldsymbol{y} = [\boldsymbol{x}^T, \boldsymbol{r}^T]^T$, we have

$$\begin{aligned}&\max_{-\boldsymbol{\rho}\leq\boldsymbol{e}\leq\boldsymbol{\rho}} \sum_{i=1}^N \left|\boldsymbol{a}_i^T\boldsymbol{y} - b_i + \Delta\boldsymbol{a}_i^T\boldsymbol{y} - \Delta b_i\right|^2 \\ &\qquad = \sum_{i=1}^N \left(\max_{-\rho_i\leq e_i\leq\rho_i} \left|\boldsymbol{a}_i^T\boldsymbol{y} - b_i + \Delta\boldsymbol{a}_i^T\boldsymbol{y} - \Delta b_i\right|\right)^2\end{aligned}$$

and

$$\boldsymbol{a}_i^T\boldsymbol{y} - b_i + \Delta\boldsymbol{a}_i^T\boldsymbol{y} - \Delta b_i = \boldsymbol{a}_i^T\boldsymbol{y} - b_i + e_i^2 - 2(d_i - r_i)e_i.$$

Hence, Problem (7) is equivalent to

$$\min_{\substack{\boldsymbol{y}=[\boldsymbol{x}^T,\boldsymbol{r}^T]^T\\ \in\mathbb{R}^{d+N}}} \sum_{i=1}^{N}\left(\max_{-\rho_i\le e_i\le\rho_i}\left|\boldsymbol{a}_i^T\boldsymbol{y}-b_i+e_i^2-2(d_i-r_i)e_i\right|\right)^2$$
$$\text{s.t.}\quad \|\boldsymbol{x}-\boldsymbol{s}_i\|=r_i \quad \text{for } i=1,\ldots,N. \tag{8}$$

In particular, both the objective function and the constraints of Problem (8) are non-convex in general. To transform (8) into a form that is more amenable to algorithmic treatment, let us first tackle the objective function. By the triangle inequality, we have

$$\begin{aligned}&\left|\boldsymbol{a}_i^T\boldsymbol{y}-b_i+e_i^2-2(d_i-r_i)e_i\right|\\ &\qquad\le\left|\boldsymbol{a}_i^T\boldsymbol{y}-b_i\right|+\left|e_i^2-2(d_i-r_i)e_i\right|.\end{aligned}$$

Hence,

$$\begin{aligned}&\max_{-\rho_i\le e_i\le\rho_i}\left|\boldsymbol{a}_i^T\boldsymbol{y}-b_i+e_i^2-2(d_i-r_i)e_i\right|\\ &\qquad\le\left|\boldsymbol{a}_i^T\boldsymbol{y}-b_i\right|+\max_{-\rho_i\le e_i\le\rho_i}\left|e_i^2-2(d_i-r_i)e_i\right|.\end{aligned} \tag{9}$$

It is elementary to verify that

$$\begin{aligned}&\max_{-\rho_i\le e_i\le\rho_i}\left|e_i^2-2(d_i-r_i)e_i\right|\\ &=\begin{cases}\max\left\{\left|\rho_i^2\pm2\rho_i(d_i-r_i)\right|,(d_i-r_i)^2\right\} & \text{if } |d_i-r_i|\le\rho_i,\\ \max\left\{\left|\rho_i^2\pm2\rho_i(d_i-r_i)\right|\right\} & \text{otherwise.}\end{cases}\end{aligned} \tag{10}$$

In fact, the above equality can be simplified as follows:

Proposition 1: The following holds:

$$\begin{aligned}\max_{-\rho_i\le e_i\le\rho_i}\left|e_i^2-2(d_i-r_i)e_i\right|&=\max\left\{\rho_i^2\pm2\rho_i(d_i-r_i)\right\}\\ &=\rho_i^2+2\rho_i|d_i-r_i|.\end{aligned} \tag{11}$$

Proof: The second equality is straightforward. To establish the first equality, consider the following cases:

Case 1: $|d_i-r_i|\le\rho_i$.

If $-\rho_i\le d_i-r_i\le 0$, then

$$\begin{aligned}&\rho_i^2-2\rho_i(d_i-r_i)\ge\left|\rho_i^2+2\rho_i(d_i-r_i)\right|,\\ &\rho_i^2-2\rho_i(d_i-r_i)\ge(d_i-r_i)^2+2(d_i-r_i)^2=3(d_i-r_i)^2.\end{aligned}$$

On the other hand, if $0\le d_i-r_i\le\rho_i$, then

$$\begin{aligned}&\rho_i^2+2\rho_i(d_i-r_i)\ge\left|\rho_i^2-2\rho_i(d_i-r_i)\right|,\\ &\rho_i^2+2\rho_i(d_i-r_i)\ge(d_i-r_i)^2+2(d_i-r_i)^2=3(d_i-r_i)^2.\end{aligned}$$

Hence, we conclude from (10) that (11) holds.

Case 2: $|d_i-r_i|>\rho_i$.

If $d_i-r_i>\rho_i$, then trivially,

$$\rho_i^2+2\rho_i(d_i-r_i)\ge\left|\rho_i^2-2\rho_i(d_i-r_i)\right|.$$

Similarly, if $d_i-r_i<-\rho_i$, then

$$\rho_i^2-2\rho_i(d_i-r_i)\ge\left|\rho_i^2+2\rho_i(d_i-r_i)\right|.$$

Using (10), this again establishes (11). ∎

Since the function

$$\boldsymbol{y}\mapsto\left|\boldsymbol{a}_i^T\boldsymbol{y}-b_i\right|+2\rho_i|d_i-r_i|+\rho_i^2$$

is non-negative and convex in $\boldsymbol{y}$ for $i=1,\ldots,N$, Proposition 1 and (9) imply that the function

$$\boldsymbol{y}\mapsto\sum_{i=1}^{N}\left(\left|\boldsymbol{a}_i^T\boldsymbol{y}-b_i\right|+2\rho_i|d_i-r_i|+\rho_i^2\right)^2 \tag{12}$$

is a *convex majorant* of the non-convex objective function of Problem (8). This motivates the following approximation of Problem (8):

$$\begin{aligned}\min_{\boldsymbol{y}=[\boldsymbol{x}^T,\boldsymbol{r}^T]^T\in\mathbb{R}^{d+N}}\quad&\sum_{i=1}^{N}\left(\left|\boldsymbol{a}_i^T\boldsymbol{y}-b_i\right|+2\rho_i|d_i-r_i|+\rho_i^2\right)^2\\ \text{s.t.}\quad&\|\boldsymbol{x}-\boldsymbol{s}_i\|=r_i\quad\text{for } i=1,\ldots,N.\end{aligned} \tag{13}$$

Although Problem (13) is still non-convex, it can be tackled by convex relaxation techniques. Indeed, by relaxing $\|\boldsymbol{x}-\boldsymbol{s}_i\|=r_i$ to $\|\boldsymbol{x}-\boldsymbol{s}_i\|\le r_i$ (for $i=1,\ldots,N$) in Problem (13) and introducing the auxiliary variables η_0 and $\boldsymbol{\eta}=[\eta_1,\ldots,\eta_N]^T$, we obtain the following second-order cone relaxation (SOCR) of Problem (13):

$$\begin{aligned}\min_{\substack{\boldsymbol{y}=[\boldsymbol{x}^T,\boldsymbol{r}^T]^T\in\mathbb{R}^{d+N}\\ \boldsymbol{\eta}\in\mathbb{R}^N,\ \eta_0\in\mathbb{R}}}\quad&\eta_0\\ \text{s.t.}\quad&\left|\boldsymbol{a}_i^T\boldsymbol{y}-b_i\right|+2\rho_i|d_i-r_i|+\rho_i^2\le\eta_i\\ &\qquad\text{for } i=1,\ldots,N, \quad\text{(14a)}\\ &\|\boldsymbol{x}-\boldsymbol{s}_i\|\le r_i\\ &\qquad\text{for } i=1,\ldots,N, \quad\text{(14b)}\\ &\|\boldsymbol{\eta}\|^2\le\eta_0. \quad\text{(14c)}\end{aligned}$$

Note that the constraint (14c) is equivalent to

$$\left\|\left[\eta_0-\frac{1}{4},\boldsymbol{\eta}^T\right]^T\right\|\le\eta_0+\frac{1}{4}$$

and hence it can be expressed as a second-order cone constraint. Also, note that if $d_i<0$, then $d_i-r_i<0$, which implies that the constraint (14a) can be simplified to $\left|\boldsymbol{a}_i^T\boldsymbol{y}-b_i\right|-2\rho_i(d_i-r_i)+\rho_i^2\le\eta_i$.

To derive a semidefinite relaxation (SDR) of Problem (13), we first observe that

$$\begin{aligned}&\left(\left|\boldsymbol{a}_i^T\boldsymbol{y}-b_i\right|+2\rho_i|d_i-r_i|+\rho_i^2\right)^2\\ &=\max\left\{\left(\pm\left(\boldsymbol{a}_i^T\boldsymbol{y}-b_i\right)\pm2\rho_i(d_i-r_i)+\rho_i^2\right)^2\right\}.\end{aligned}$$

Hence, Problem (13) is equivalent to

$$\begin{aligned}\min_{\substack{\boldsymbol{y}=[\boldsymbol{x}^T,\boldsymbol{r}^T]^T\in\mathbb{R}^{d+N},\\ \boldsymbol{\tau}\in\mathbb{R}^N}}\quad&\sum_{i=1}^{N}\tau_i\\ \text{s.t.}\quad&\left(\boldsymbol{a}_i^T\boldsymbol{y}-b_i+2\rho_i(d_i-r_i)+\rho_i^2\right)^2\le\tau_i\\ &\qquad\text{for } i=1,\ldots,N, \quad\text{(15a)}\\ &\left(\boldsymbol{a}_i^T\boldsymbol{y}-b_i-2\rho_i(d_i-r_i)+\rho_i^2\right)^2\le\tau_i\\ &\qquad\text{for } i=1,\ldots,N, \quad\text{(15b)}\\ &\left(-\boldsymbol{a}_i^T\boldsymbol{y}+b_i+2\rho_i(d_i-r_i)+\rho_i^2\right)^2\le\tau_i\\ &\qquad\text{for } i=1,\ldots,N, \quad\text{(15c)}\\ &\left(-\boldsymbol{a}_i^T\boldsymbol{y}+b_i-2\rho_i(d_i-r_i)+\rho_i^2\right)^2\le\tau_i\\ &\qquad\text{for } i=1,\ldots,N, \quad\text{(15d)}\\ &\|\boldsymbol{x}-\boldsymbol{s}_i\|=r_i\quad\text{for } i=1,\ldots,N, \quad\text{(15e)}\end{aligned}$$

where $\boldsymbol{\tau} = [\tau_1, \ldots, \tau_N]^T$. Now, let $\boldsymbol{v}_j = [\boldsymbol{0}_{1\times(j-1)}, 1, \boldsymbol{0}_{1\times(d+N-j)}]^T$ be the jth basis vector in $\mathbb{R}^{d+N}$, $\boldsymbol{Y} = \boldsymbol{y}\boldsymbol{y}^T$, and

$$\begin{aligned}
&\boldsymbol{c}_i = \boldsymbol{a}_i + 2\rho_i \boldsymbol{v}_{d+i}, \quad \bar{\boldsymbol{c}}_i = \boldsymbol{a}_i - 2\rho_i \boldsymbol{v}_{d+i},\\
&\boldsymbol{C}_i = \boldsymbol{c}_i\boldsymbol{c}_i^T, \quad \bar{\boldsymbol{C}}_i = \bar{\boldsymbol{c}}_i\bar{\boldsymbol{c}}_i^T,\\
&\kappa_i = \rho_i^2 + 2d_i\rho_i + b_i, \quad \bar{\kappa}_i = \rho_i^2 + 2d_i\rho_i - b_i,\\
&\theta_i = \rho_i^2 - 2d_i\rho_i + b_i, \quad \bar{\theta}_i = \rho_i^2 - 2d_i\rho_i - b_i.
\end{aligned}$$

Since $\boldsymbol{y} = \left[\boldsymbol{x}^T, \boldsymbol{r}^T\right]^T$, the constraints (15a)–(15d) can be expressed as

$$\operatorname{tr}\left(\bar{\boldsymbol{C}}_i\boldsymbol{Y}\right) + 2\bar{\kappa}_i\bar{\boldsymbol{c}}_i^T\boldsymbol{y} + \bar{\kappa}_i^2 \le \tau_i, \tag{16a}$$

$$\operatorname{tr}\left(\boldsymbol{C}_i\boldsymbol{Y}\right) + 2\bar{\theta}_i\boldsymbol{c}_i^T\boldsymbol{y} + \bar{\theta}_i^2 \le \tau_i, \tag{16b}$$

$$\operatorname{tr}\left(\boldsymbol{C}_i\boldsymbol{Y}\right) - 2\kappa_i\boldsymbol{c}_i^T\boldsymbol{y} + \kappa_i^2 \le \tau_i, \tag{16c}$$

$$\operatorname{tr}\left(\bar{\boldsymbol{C}}_i\boldsymbol{Y}\right) - 2\theta_i\bar{\boldsymbol{c}}_i^T\boldsymbol{y} + \theta_i^2 \le \tau_i, \tag{16d}$$

while the constraint (15e) can be expressed as

$$\operatorname{tr}\left(\boldsymbol{Q}_i\boldsymbol{Y}\right) - 2\bar{\boldsymbol{s}}_i^T\boldsymbol{y} + \|\boldsymbol{s}_i\|^2 = 0, \tag{17}$$

where

$$\begin{aligned}
\boldsymbol{Q}_i &= \begin{bmatrix} \boldsymbol{I}_d & \boldsymbol{0}_{d\times N} \\ \boldsymbol{0}_{N\times d} & \boldsymbol{D}_i \end{bmatrix} \in \mathbb{S}^{d+N},\\
\boldsymbol{D}_i &= \operatorname{Diag}(0, \ldots, 0, \underbrace{-1}_{i}, 0, \ldots, 0) \in \mathbb{S}^N,\\
\bar{\boldsymbol{s}}_i &= \left[\boldsymbol{s}_i^T, \boldsymbol{0}_{1\times N}\right]^T \in \mathbb{R}^{d+N}.
\end{aligned}$$

Moreover, we have the equivalence

$$\begin{aligned}
&\boldsymbol{Y} = \boldsymbol{y}\boldsymbol{y}^T \quad \Longleftrightarrow\\
&\boldsymbol{Z} = \begin{bmatrix} \boldsymbol{Y} & \boldsymbol{y} \\ \boldsymbol{y}^T & 1 \end{bmatrix} \succeq \boldsymbol{0}_{(d+N+1)\times(d+N+1)}, \quad \operatorname{rank}(\boldsymbol{Z}) = 1.
\end{aligned} \tag{18}$$

Thus, by dropping the non-convex rank constraint $\operatorname{rank}(\boldsymbol{Z}) = 1$ in (18) (cf. [31]), we obtain the following SDR of Problem (13):

$$\begin{aligned}
\min_{\substack{\boldsymbol{Y}\in\mathbb{S}^{d+N}\\ \boldsymbol{y}\in\mathbb{R}^{d+N},\,\boldsymbol{\tau}\in\mathbb{R}^N}} \quad & \sum_{i=1}^N \tau_i\\
\text{s.t.} \quad & \text{(16a)–(16d), (17)},\\
& \begin{bmatrix} \boldsymbol{Y} & \boldsymbol{y} \\ \boldsymbol{y}^T & 1 \end{bmatrix} \succeq \boldsymbol{0}_{(d+N+1)\times(d+N+1)}.
\end{aligned} \tag{19}$$

IV. Analysis of the Convex Approximations

In the previous section, we tackle the non-convex RLS problem (7) in two steps. First, we replace the non-convex objective function of Problem (7) by the convex majorant (12). Then, we apply convex relaxation techniques to the resulting problem (i.e., Problem (13)), thereby leading to the SOCR-based and SDR-based approximation methods (14) and (19) for the RLS problem (7). In this section, we conduct a theoretical analysis of this two-step approach. Specifically, we first identify the conditions under which the RLS problem (7) and the convex majorant-based approximation (13) are equivalent and interpret them in the context of NLOS TDOA-based localization. Then, we study the relative tightness of the SOCR (14) and the SDR (19). Contrary to what one would expect, we show that the latter is actually not tighter than the former. Motivated by this result, we proceed to develop a refined SDR (see (21) below), which is provably tighter than the SOCR (14). Next, we analyze the computational complexity of the proposed convex relaxation-based approximation methods. Lastly, we establish sufficient conditions for the SOCR (14) and the refined SDR (21) to yield a unique localization of the source and discuss how these conditions can be verified in practice.

A. Exactness Analysis

Since the objective function of the RLS problem (7), or equivalently, that of Problem (8), is non-convex, we propose in Section III to approximate the ith summand of the latter, namely

$$S_i(\boldsymbol{y}) = \max_{-\rho_i\le e_i\le\rho_i} \left|\boldsymbol{a}_i^T\boldsymbol{y} - b_i + e_i^2 - 2(d_i - r_i)e_i\right|,$$

by the convex majorant

$$S_i^+(\boldsymbol{y}) = \left|\boldsymbol{a}_i^T\boldsymbol{y} - b_i\right| + 2\rho_i|d_i - r_i| + \rho_i^2,$$

where $i = 1, \ldots, N$ and $\boldsymbol{y} = [\boldsymbol{x}^T, \boldsymbol{r}^T]^T$. To understand when such approximation is exact, let us first derive an explicit expression for $S_i(\boldsymbol{y})$.

Proposition 2: The following holds for $i = 1, \ldots, N$:

$$\begin{aligned}
S_i(\boldsymbol{y}) &= \max_{-\rho_i\le e_i\le\rho_i} \left|\boldsymbol{a}_i^T\boldsymbol{y} - b_i + e_i^2 - 2(d_i - r_i)e_i\right|\\
&= \begin{cases}
\boldsymbol{a}_i^T\boldsymbol{y} - b_i + 2\rho_i|d_i - r_i| + \rho_i^2\\
\qquad \text{if } \boldsymbol{a}_i^T\boldsymbol{y} - b_i \ge 0,\\
\max\left\{\boldsymbol{a}_i^T\boldsymbol{y} - b_i + 2\rho_i|d_i - r_i| + \rho_i^2,\right.\\
\qquad \left.(d_i - r_i)^2 - \left(\boldsymbol{a}_i^T\boldsymbol{y} - b_i\right)\right\}\\
\qquad \text{if } \boldsymbol{a}_i^T\boldsymbol{y} - b_i < 0 \text{ and } |d_i - r_i| \le \rho_i,\\
\max\left\{\left|\boldsymbol{a}_i^T\boldsymbol{y} - b_i \pm 2\rho_i(d_i - r_i) + \rho_i^2\right|\right\}\\
\qquad \text{if } \boldsymbol{a}_i^T\boldsymbol{y} - b_i < 0 \text{ and } |d_i - r_i| > \rho_i.
\end{cases}
\end{aligned}$$

Since the proof of Proposition 2 is rather tedious, we relegate it to the Appendix. Now, armed with Proposition 2, we can prove the following result:

Proposition 3: Consider a fixed $i \in \{1, \ldots, N\}$. If $\rho_i = 0$, then $S_i(\boldsymbol{y}) = S_i^+(\boldsymbol{y})$. Otherwise, we have $S_i(\boldsymbol{y}) = S_i^+(\boldsymbol{y})$ if and only if $\boldsymbol{a}_i^T\boldsymbol{y} - b_i \ge 0$.

Proof: The claim for the case where $\rho_i = 0$ is trivial. Hence, we shall focus on the case where $\rho_i > 0$. Suppose that $\boldsymbol{a}_i^T\boldsymbol{y} - b_i \ge 0$. Then, Proposition 2 yields

$$\begin{aligned}
S_i(\boldsymbol{y}) &= \boldsymbol{a}_i^T\boldsymbol{y} - b_i + 2\rho_i|d_i - r_i| + \rho_i^2\\
&= \left|\boldsymbol{a}_i^T\boldsymbol{y} - b_i\right| + 2\rho_i|d_i - r_i| + \rho_i^2\\
&= S_i^+(\boldsymbol{y}).
\end{aligned}$$

Conversely, suppose that $\boldsymbol{a}_i^T\boldsymbol{y} - b_i < 0$. Consider the following cases:

Case 1: $|d_i - r_i| \le \rho_i$.

By Proposition 2, we have

$$S_i(\boldsymbol{y}) = \max\big\{\boldsymbol{a}_i^T\boldsymbol{y} - b_i + 2\rho_i|d_i - r_i| + \rho_i^2, \\ (d_i - r_i)^2 - \big(\boldsymbol{a}_i^T\boldsymbol{y} - b_i\big)\big\}.$$

It is clear that $\boldsymbol{a}_i^T\boldsymbol{y} - b_i + 2\rho_i|d_i - r_i| + \rho_i^2 < S_i^+(\boldsymbol{y})$. Moreover, if $|d_i - r_i| = 0$, then $(d_i - r_i)^2 - (\boldsymbol{a}_i^T\boldsymbol{y} - b_i) = \big|\boldsymbol{a}_i^T\boldsymbol{y} - b_i\big| < S_i^+(\boldsymbol{y})$. Otherwise, we have $|d_i - r_i| > 0$, which implies that

$$(d_i - r_i)^2 - (\boldsymbol{a}_i^T\boldsymbol{y} - b_i) \le \rho_i^2 + \big|\boldsymbol{a}_i^T\boldsymbol{y} - b_i\big| < S_i^+(\boldsymbol{y}).$$

Hence, we conclude that $S_i(\boldsymbol{y}) < S_i^+(\boldsymbol{y})$ in this case.

Case 2: $|d_i - r_i| > \rho_i$.

Proposition 2 states that

$$S_i(\boldsymbol{y}) = \max\big\{\big|\boldsymbol{a}_i^T\boldsymbol{y} - b_i \pm 2\rho_i(d_i - r_i) + \rho_i^2\big|\big\}$$

in this case. Suppose that $d_i - r_i > \rho_i > 0$. Then, since $\boldsymbol{a}_i^T\boldsymbol{y} - b_i < 0$ and $2\rho_i(d_i - r_i) > 0$, we have

$$\big|\boldsymbol{a}_i^T\boldsymbol{y} - b_i + 2\rho_i(d_i - r_i) + \rho_i^2\big| < S_i^+(\boldsymbol{y})$$

and

$$\big|\boldsymbol{a}_i^T\boldsymbol{y} - b_i - 2\rho_i(d_i - r_i) + \rho_i^2\big| < S_i^+(\boldsymbol{y}).$$

It follows that $S_i(\boldsymbol{y}) < S_i^+(\boldsymbol{y})$. The case where $d_i - r_i < -\rho_i < 0$ can be handled in a similar manner. ■

Proposition 3 characterizes the conditions under which the convex majorant approximation (12) of the non-convex objective function of the RLS problem (7) is *exact*. To see its implications on the efficacy of the proposed approach, let us consider a fixed $i \in \{1, \ldots, N\}$ and use (2), (5), (6) to compute

$$\begin{aligned}\boldsymbol{a}_i^T\boldsymbol{y} - b_i &= 2(\boldsymbol{s}_0 - \boldsymbol{s}_i)^T\boldsymbol{x} - 2d_i\|\boldsymbol{x} - \boldsymbol{s}_i\| \\ &\quad - \|\boldsymbol{s}_0\|^2 + \|\boldsymbol{s}_i\|^2 + d_i^2 \\ &= (d_i - \|\boldsymbol{x} - \boldsymbol{s}_i\|)^2 - \|\boldsymbol{x}\|^2 + 2\boldsymbol{s}_0^T\boldsymbol{x} - \|\boldsymbol{s}_0\|^2 \\ &= (n_i + e_i)^2 - 2\|\boldsymbol{x} - \boldsymbol{s}_0\|(n_i + e_i).\end{aligned}$$

This shows that the sign of $\boldsymbol{a}_i^T\boldsymbol{y} - b_i$ is completely determined by that of $(n_i + e_i)^2 - 2\|\boldsymbol{x} - \boldsymbol{s}_0\|(n_i + e_i)$. In particular, we have the following two scenarios:

Scenario A: $n_i + e_i \le 0$ or $n_i + e_i \ge 2\|\boldsymbol{x} - \boldsymbol{s}_0\|$.

From the measurement model (1), we see that this scenario occurs, e.g., when the path from the source to the reference sensor is highly NLOS (so that the estimate of $\|\boldsymbol{x}^* - \boldsymbol{s}_0\|$ is significantly positively biased, where $\boldsymbol{x}^* \in \mathbb{R}^d$ is the true location of the source) and the path from the source to the ith sensor is (almost) LOS (so that the estimate of $\|\boldsymbol{x}^* - \boldsymbol{s}_i\|$ is lightly positively biased), or when the path from the source to the reference sensor is (almost) LOS and the path from the source to the ith sensor is highly NLOS. Note that in this scenario, we have $\boldsymbol{a}_i^T\boldsymbol{y} - b_i \ge 0$. Thus, Proposition 3 suggests that our approach should perform well. This is corroborated by our simulation results; see Scenarios 1, 2, 4, and 7 in Section V-A.

Scenario B: $0 < n_i + e_i < 2\|\boldsymbol{x} - \boldsymbol{s}_0\|$.

By reasoning in a similar manner as above, we see that this scenario occurs, e.g., when the path from the source to the reference sensor is (almost) LOS and the path from the source to the ith sensor is mildly NLOS (so that $n_i + e_i < 2\|\boldsymbol{x} - \boldsymbol{s}_0\|$). In this scenario, we have $\boldsymbol{a}_i^T\boldsymbol{y} - b_i < 0$. Thus, Proposition 3 suggests that our approach may not perform so well; see Scenarios 2, 3, 6, and 9 in Section V-A.

B. Relative Tightness Analysis

In Section III, we propose two convex relaxations of Problem (13), namely the SOCR (14) and the SDR (19). It is natural to ask which relaxation is tighter. Roughly speaking, if the SDR (19) is tighter than the SOCR (14), then the feasible set of (19) is contained in that of (14), which implies that the optimal value of (14) is at most that of (19). This motivates us to formalize the tightness question as follows:

Question (Q): Given an arbitrary feasible solution $(\bar{\boldsymbol{Y}}, \bar{\boldsymbol{y}}, \bar{\boldsymbol{\tau}})$ to the SDR (19) with objective value $v_{\text{SDR}} = \sum_{i=1}^N \bar{\tau}_i$, does there exist a feasible solution $(\boldsymbol{y}', \boldsymbol{\eta}', \eta_0')$ to the SOCR (14) with objective value $v_{\text{SOCR}} = \eta_0' \le v_{\text{SDR}}$?

In view of the works [23]–[25], one would expect that the answer to (Q) is affirmative; i.e., the SDR (19) is tighter than the SOCR (14). However, this is not the case, as the following example shows:

Example 1: Consider 5 sensors located at $\boldsymbol{s}_0 = [0, 0]^T$, $\boldsymbol{s}_1 = [10, 0]^T$, $\boldsymbol{s}_2 = [0, 10]^T$, $\boldsymbol{s}_3 = [-10, 0]^T$, and $\boldsymbol{s}_4 = [0, -10]^T$, respectively, with $\boldsymbol{s}_0$ being the reference sensor. Suppose that the source is located at $\boldsymbol{x}^* = [7, 6]^T$. The exact (i.e., without measurement noise and NLOS errors) and noisy range-difference measurements are shown in Table I,[1] while the optimal values of the SOCR (14) and the SDR (19), as well as their corresponding estimates of $\boldsymbol{x}^*$, are shown in Table II.

TABLE I
EXACT AND NOISY RANGE-DIFFERENCE MEASUREMENTS

	d_1	d_2	d_3	d_4
exact	-2.5113	-1.1573	8.8082	8.2447
noisy	-5.0683	-2.7352	6.0505	6.3506

Clearly, there is no feasible solution to the SOCR (14) that has an objective value of at most 11260, which implies that the SDR (19) is not tighter than the SOCR (14). ■

Given the above example, an immediate question is whether one can derive a tighter relaxation than the SOCR (14). The answer is affirmative. To motivate the development, observe that given any feasible solution $(\bar{\boldsymbol{Y}}, \bar{\boldsymbol{y}}, \bar{\boldsymbol{\tau}})$ to the SDR (19) with $\bar{\boldsymbol{y}} = \big[\bar{\boldsymbol{x}}^T, \bar{\boldsymbol{r}}^T\big]^T$, the constraint (17) and

$$\begin{bmatrix} \boldsymbol{Y} & \boldsymbol{y} \\ \boldsymbol{y}^T & 1 \end{bmatrix} \succeq \boldsymbol{0}_{(d+N+1)\times(d+N+1)} \quad \Longleftrightarrow \quad \boldsymbol{Y} \succeq \boldsymbol{y}\boldsymbol{y}^T$$

imply that

$$\|\bar{\boldsymbol{x}} - \boldsymbol{s}_i\|^2 \le \bar{Y}_{d+i,d+i} \quad \text{and} \quad \bar{r}_i^2 \le \bar{Y}_{d+i,d+i} \quad \text{for } i = 1, \ldots, N. \tag{20}$$

Hence, the first inequality in (20) is always weaker than the inequality $\|\bar{\boldsymbol{x}} - \boldsymbol{s}_i\| \le \bar{r}_i$. Note that the latter is present in the

[1]The measurement noise and NLOS errors are generated according to the procedure described in Section V-A, where we set $\sigma = 0.3$ and $\omega_i = 3$ for $i = 0, 1, \ldots, 4$.

TABLE II
OPTIMAL VALUES AND SOURCE LOCATION ESTIMATES OF THE VARIOUS FORMULATIONS

	SOCR (14)	SDR (19)	Refined SDR (21)
opt. value	47551	11260	60672
loc. estimate	$[8.6185, 6.6479]^T$	$[0.1049, 2.1406]^T$	$[7.6458, 5.8385]^T$

SOCR (14). This suggests that we can tighten the SDR (19) by including this latter inequality; i.e., consider the refined SDR

$$\begin{aligned} \min_{\substack{\boldsymbol{Y}\in\mathbb{S}^{d+N} \\ \boldsymbol{y}=[\boldsymbol{x}^T,\boldsymbol{r}^T]^T\in\mathbb{R}^{d+N},\,\boldsymbol{\tau}\in\mathbb{R}^N}} \quad & \sum_{i=1}^N \tau_i \\ \text{s.t.} \quad & \text{(16a)–(16d), (17)}, \\ & \|\boldsymbol{x}-\boldsymbol{s}_i\| \le r_i, \text{ for } i=1,\ldots,N, \qquad (21a) \\ & \begin{bmatrix} \boldsymbol{Y} & \boldsymbol{y} \\ \boldsymbol{y}^T & 1 \end{bmatrix} \succeq \boldsymbol{0}_{(d+N+1)\times(d+N+1)}. \qquad (21b) \end{aligned}$$

As it turns out, the inclusion of the set of constraints (21a) is sufficient to guarantee that the refined SDR (21) is tighter than the SOCR (14):

Theorem 1: Let $(\bar{\boldsymbol{Y}}, \bar{\boldsymbol{y}}, \bar{\boldsymbol{\tau}})$ be a feasible solution to the refined SDR (21) with objective value $v_{\text{SDR}} = \sum_{i=1}^N \bar{\tau}_i$, where $\bar{\boldsymbol{y}} = \left[\bar{\boldsymbol{x}}^T, \bar{\boldsymbol{r}}^T\right]^T$. Then, the solution $(\bar{\boldsymbol{y}}, \bar{\boldsymbol{\eta}}, \bar{\eta}_0)$, where

$$\bar{\eta}_i = \left|\boldsymbol{a}_i^T\bar{\boldsymbol{y}} - b_i\right| + 2\rho_i|d_i - \bar{r}_i| + \rho_i^2 \quad \text{for } i=1,\ldots,N$$

and $\bar{\eta}_0 = \|\bar{\boldsymbol{\eta}}\|^2$, is feasible for the SOCR (14) and has objective value $v_{\text{SOCR}} = \bar{\eta}_0 \le v_{\text{SDR}}$.

Proof: It is straightforward to verify that $(\bar{\boldsymbol{y}}, \bar{\boldsymbol{\eta}})$ satisfies the constraint (14a). Moreover, since $\bar{\boldsymbol{y}}$ satisfies the constraint (21a), it also satisfies the constraint (14b). Finally, by construction, $(\bar{\boldsymbol{\eta}}, \bar{\eta}_0)$ satisfies the constraint (14c). Hence, $(\bar{\boldsymbol{y}}, \bar{\boldsymbol{\eta}}, \bar{\eta}_0)$ is feasible for (14).

Now, since $\boldsymbol{C}_i, \bar{\boldsymbol{C}}_i \succeq \boldsymbol{0}_{(d+N)\times(d+N)}$ for $i=1,\ldots,N$, by (16a)–(16d) and (21b), we have

$$\bar{\tau}_i \ge \left(\left|\boldsymbol{a}_i^T\bar{\boldsymbol{y}} - b_i\right| + 2\rho_i|d_i - \bar{r}_i| + \rho_i^2\right)^2 = \bar{\eta}_i^2 \quad \text{for } i=1,\ldots,N.$$

It follows that

$$v_{\text{SDR}} = \sum_{i=1}^n \bar{\tau}_i \ge \sum_{i=1}^n \bar{\eta}_i^2 = \bar{\eta}_0 = v_{\text{SOCR}},$$

as desired. ∎

The reader may notice that the conclusion of Theorem 1 remains valid even without the constraint (17). Nevertheless, its inclusion in the refined SDR (21) serves to further tighten the relaxation.

As an illustration of Theorem 1, consider Example 1 again. From Table II, we see that the optimal value of the refined SDR (21) is higher than that of the SOCR (14). Moreover, the estimate of $\boldsymbol{x}^*$ produced by (21) is closer to the truth than that produced by (14).

C. Complexity Analysis

It is well-known that both the SOCR (14) and the refined SDR (21) can be solved in polynomial time by a standard interior-point method; see, e.g., [21, Lecture 6]. To compare their worst-case computational complexities, we first recall that the complexity of a generic interior-point method for solving a mixed second-order cone and semidefinite cone programming problem is on the order of

$$\sqrt{\mu}\cdot\left(m\sum_{i=1}^{N_{soc}}\left(n_i^{soc}\right)^2 + m^2\sum_{i=1}^{N_{sd}}\left(n_i^{sd}\right)^2 + m\sum_{i=1}^{N_{sd}}\left(n_i^{sd}\right)^3 + m^3\right)\cdot\ln(1/\epsilon),$$

where m is the number of variables, N_{SOC} (resp. N_{SD}) is the number of second-order cone (resp. semidefinite cone) constraints, n_i^{SOC} (resp. n_i^{SD}) is the dimension of the ith second-order cone (resp. semidefinite cone),

$$\mu = \sum_{i=1}^{N_{\text{SD}}} n_i^{\text{SD}} + 2N_{\text{SOC}}$$

is the so-called barrier parameter and measures the geometric complexities of the cones involved, and $\epsilon > 0$ is the solution precision; see, e.g., [21, Lecture 6] or [32, Section V-A]. Now, the SOCR (14) has $d+2N+1$ variables, $4N$ semidefinite cone constraints of size 1 (corresponding to the $4N$ linear inequality constraints (14a)), N second-order cone constraints of size $d+1$ (corresponding to (14b)), and 1 second-order cone constraint of size $N+2$ (corresponding to (14c)). Hence, its worst-case complexity is on the order of

$$\sqrt{N}\cdot\left[N(d+N)(d^2+N) + (d+N)^3\right]\cdot\ln(1/\epsilon).$$

On the other hand, the refined SDR (21) has $\binom{d+N+1}{2}+d+2N$ variables, $6N$ semidefinite cone constraints of size 1 (corresponding to the $6N$ linear inequality constraints (16a)–(16d), (17)), N second-order cone constraints of size $d+1$ (corresponding to (21a)), and 1 semidefinite cone constraint of size $d+N+1$ (corresponding to (21b)). Hence, its worst-case complexity is on the order of

$$(d+N)^{6.5}\cdot\ln(1/\epsilon).$$

The above analysis and the results in Section IV-B show that there is a tradeoff between performance and computational complexity in the SOCR (14) and the refined SDR (21). It should be noted, however, that the above complexity bounds are based on a worst-case analysis. In practice, the structure of the constraint matrices often allows the refined SDR (21) to be solved much more efficiently.

D. Unique Localizability Analysis

Another fundamental issue concerning the convex relaxations (14) and (21) is whether they can uniquely localize the source. Specifically, we say that the SOCR (14) (resp. the refined SDR (21)) uniquely localizes the source if the $\boldsymbol{x}$-component of the solution is invariant over the set of optimal solutions to (14) (resp. (21)). In this subsection, we study conditions under which the convex relaxations (14) and (21) can uniquely localize the source. We begin with the following proposition:

Proposition 4: Suppose there exists an $i \in \{1, \ldots, N\}$ such that

$$\|\boldsymbol{x}^* - \boldsymbol{s}_i\| = r_i^*$$

holds for all optimal solutions $(\boldsymbol{y}^*, \boldsymbol{\eta}^*, \eta_0^*)$ (resp. $(\boldsymbol{Y}^*, \boldsymbol{y}^*, \boldsymbol{\tau}^*)$) to (14) (resp. (21)), where $\boldsymbol{y}^* = \left[(\boldsymbol{x}^*)^T, (\boldsymbol{r}^*)^T\right]^T$. Then, the SOCR (14) (resp. the refined SDR (21)) uniquely localizes the source.

Proof: We shall establish the proposition for the SOCR (14). The argument for the refined SDR (21) is similar. Let $(\boldsymbol{y}^*, \boldsymbol{\eta}^*, \eta_0^*)$ and $(\bar{\boldsymbol{y}}^*, \bar{\boldsymbol{\eta}}^*, \eta_0^*)$ be two optimal solutions to (14), with $\boldsymbol{y}^* = \left[(\boldsymbol{x}^*)^T, (\boldsymbol{r}^*)^T\right]^T$ and $\bar{\boldsymbol{y}}^* = \left[(\bar{\boldsymbol{x}}^*)^T, (\bar{\boldsymbol{r}}^*)^T\right]^T$ (note that η_0^* is the optimal value and hence must be the same for the two optimal solutions). Since the set of optimal solutions to (14) is convex, the solution

$$\left(\frac{\boldsymbol{y}^* + \bar{\boldsymbol{y}}^*}{2}, \frac{\boldsymbol{\eta}^* + \bar{\boldsymbol{\eta}}^*}{2}, \eta_0\right)$$

is also optimal for (14). By assumption, we have

$$\|\boldsymbol{x}^* - \boldsymbol{s}_i\| = r_i^*, \quad \|\bar{\boldsymbol{x}}^* - \boldsymbol{s}_i\| = \bar{r}_i^*,$$
$$\left\|\frac{\boldsymbol{x}^* + \bar{\boldsymbol{x}}^*}{2} - \boldsymbol{s}_i\right\| = \frac{r_i^* + \bar{r}_i^*}{2}$$

for some $i \in \{1, \ldots, N\}$. This implies that

$$\left\|\frac{\boldsymbol{x}^* - \boldsymbol{s}_i}{2} + \frac{\bar{\boldsymbol{x}}^* - \boldsymbol{s}_i}{2}\right\| = \frac{\|\boldsymbol{x}^* - \boldsymbol{s}_i\|}{2} + \frac{\|\bar{\boldsymbol{x}}^* - \boldsymbol{s}_i\|}{2}.$$

Since the Euclidean norm is strictly convex, we conclude that $\boldsymbol{x}^* - \boldsymbol{s}_i = \bar{\boldsymbol{x}}^* - \boldsymbol{s}_i$, or equivalently, $\boldsymbol{x}^* = \bar{\boldsymbol{x}}^*$, as desired. ■

Although Proposition 4 provides a sufficient condition for unique localization by the SOCR (14) and the refined SDR (21), the condition is difficult to verify both analytically and computationally. Nevertheless, it can be used to establish another sufficient condition that is efficiently verifiable. Specifically, consider the following proposition:

Proposition 5: Let $\boldsymbol{Y} \in \mathbb{S}^{d+N}$ be decomposed as

$$\boldsymbol{Y} = \begin{bmatrix} \boldsymbol{Y}_{11} & \boldsymbol{Y}_{12} \\ \boldsymbol{Y}_{12}^T & \boldsymbol{Y}_{22} \end{bmatrix},$$

where $\boldsymbol{Y}_{11} \in \mathbb{S}^d$, $\boldsymbol{Y}_{12} \in \mathbb{R}^{d \times N}$, and $\boldsymbol{Y}_{22} \in \mathbb{S}^N$. Suppose that every optimal solution $(\boldsymbol{Y}^*, \boldsymbol{y}^*, \boldsymbol{\tau}^*)$ to the refined SDR (21) satisfies $\mathrm{rank}(\boldsymbol{Y}_{11}^*) \leq 1$. Then, the refined SDR (21) uniquely localizes the source.

Proof: The constraint (21b) implies that $\boldsymbol{Y}_{11}^* \succeq \boldsymbol{x}^*(\boldsymbol{x}^*)^T$, where $\boldsymbol{y}^* = \left[(\boldsymbol{x}^*)^T, (\boldsymbol{r}^*)^T\right]^T$. Since $\mathrm{rank}(\boldsymbol{Y}_{11}^*) \leq 1$, we have $\boldsymbol{Y}_{11}^* = \boldsymbol{x}^*(\boldsymbol{x}^*)^T$. This, together with (17), implies that $\|\boldsymbol{x}^* - \boldsymbol{s}_i\|^2 = Y_{d+i,d+i}^*$ for $i = 1, \ldots, N$. However, by (21a) and (21b), we have $\|\boldsymbol{x}^* - \boldsymbol{s}_i\|^2 \leq (r_i^*)^2$ and $Y_{d+i,d+i}^* \geq (r_i^*)^2$. Hence, we have $Y_{d+i,d+i}^* = (r_i^*)^2$, which, by Proposition 4, implies that the refined SDR (21) uniquely localizes the source. ■

We claim that the sufficient condition stated in Proposition 5 can be efficiently verified *a posteriori*. Indeed, it is known that standard interior-point methods for solving semidefinite programs will always return a solution with the highest rank [33]; cf. [23]. Hence, once we solve the refined SDR (21) by an interior-point method and obtain an optimal solution $(\boldsymbol{Y}^*, \boldsymbol{y}^*, \boldsymbol{\tau}^*)$, it suffices to check if the rank condition $\mathrm{rank}(\boldsymbol{Y}_{11}^*) \leq 1$ is satisfied. If so, then every optimal solution to (21) will satisfy the same rank condition, which implies that the sufficient condition stated in Proposition 5 holds. As our simulation results in the next section show, the rank condition is usually satisfied.

V. Numerical Results

In this section, we use both synthetic and real data to test the performance of the proposed SOCR- and SDR-based robust methods and three non-robust methods: the SDR-based method in [27][2] (cf. [34]), the weighted least squares (WLS)-based method in [35] (see also [36] and [37]), and the reduced-complexity SDR-based method in [38]. In the following, we use "SDR-Non-Robust", "WLS-Non-Robust", and "RC-SDR-Non-Robust" to denote the methods in [27], [35], and [38], respectively, and use "SOCR-Robust" and "SDR-Robust" to denote the proposed SOCR- and SDR-based robust methods (14) and (21), respectively. All methods are implemented using MATLAB R2012b on a DELL personal computer equipped with a 3.3GHz Intel(R) Core(TM) i5-2500 CPU and 8GB RAM. The SOCR and SDR are solved using the MATLAB toolbox `CVX` [22], and the solver is SDPT3 [39].

A. Performance Evaluation Using Synthetic Data

Let us begin by describing the experimental setup used in this subsection. We assume that the reference sensor is located at $\boldsymbol{s}_0 = [0, 0]^T$, and the other N sensors are uniformly placed on a circle with center $(0, 0)$ and radius 10; i.e.,

$$\boldsymbol{s}_i = 10\left[\cos\frac{2\pi(i-1)}{N}, \sin\frac{2\pi(i-1)}{N}\right]^T \quad \text{for } i = 1, \ldots, N.$$

The source location is chosen uniformly at random from a disk centered at $(0, 0)$ with radius 15. It is worth noting that the source may lie outside of the convex hull of the sensors. The range-difference measurements are generated according to (2), where $e_i = U_i - U_0$ for $i = 1, \ldots, N$, and U_i is uniformly distributed between 0 and ω_i for $i = 0, 1, \ldots, N$. Here, ω_0 and ω_i (for $i = 1, \ldots, N$) are the upper bounds on the NLOS errors in the range measurements between the source and the reference sensor and between the source and the ith sensor, respectively. In particular, we have $|e_i| \leq \rho_i = \max\{\omega_0, \omega_i\}$ for $i = 1, \ldots, N$. The measurement noise vector $\boldsymbol{n} = [n_1, \ldots, n_N]^T$ is generated according to a Gaussian distribution with mean

[2]In our simulations, we actually use a strengthened version of the SDR-based method in [27], which is obtained by adding the valid inequalities $t_i \geq 0$ for $i = 1, \ldots, M$ to the SDR (20) in [27].

zero and covariance matrix $\mathbf{\Sigma} = 0.5\sigma^2\left(\boldsymbol{I}_N + \mathbf{1}_N\mathbf{1}_N^T\right)$, where $\sigma > 0$ is a parameter controlling the power of the measurement noise. The localization performance is measured by the root mean square error (RMSE) criterion, which is defined as

$$\text{RMSE} = \sqrt{\frac{1}{M}\sum_{i=1}^{M}\|\hat{\boldsymbol{x}}_i - \boldsymbol{x}_i^*\|^2}. \tag{22}$$

Here, M is the number of Monte Carlo (MC) runs; $\hat{\boldsymbol{x}}_i$ and $\boldsymbol{x}_i^*$ are the estimated and true location of the source in the ith run, respectively. In our experiments, we use $M = 3000$ MC runs.

1) Performance Comparison: To evaluate the performance of the various methods, we consider nine different scenarios, which we divide into three groups. In the first group of three scenarios, we test how the signs and magnitudes of NLOS errors in the TDOA measurements (i.e., the e_i's) affect the localization performance. This is to validate the conclusions obtained from the exactness analysis in Section IV-A. In the second group of three scenarios, we investigate how the power of measurement noise (i.e., σ^2) affects the localization performance under different levels of NLOS errors in the TDOA measurements. In the last group of three scenarios, we examine how the number of sensors (i.e., $N+1$) affects the localization performance under different levels of NLOS errors in the TDOA measurements.

Group I: Varying the Signs and Magnitudes of NLOS Errors in the TDOA Measurements

In this group of experiments, we fix the number of sensors at 5 (and hence $N = 4$) and set $\sigma = 0.3$.

- *Scenario 1*: In this scenario, we set $\omega_0 = 5\alpha$ and $\omega_i = 0.5$ for $i = 1, \ldots, 4$, where α varies from 0.1 to 1. In particular, the NLOS effect on the path from the source to the reference sensor is likely to be more pronounced than those from the source to the other sensors. Thus, the e_i's are likely to be negative. According to the analysis in Section IV-A, the convex majorant approximation (12) of the non-convex objective function of the RLS problem (7) should be exact under such setting, which suggests that the robust methods should perform well. As Fig. 1 shows, this is indeed the case.
- *Scenario 2*: Fig. 2 shows the simulation results when $\omega_0 = 3$ and $\omega_i = 5\alpha$ for $i = 1, \ldots, 4$, where α again varies from 0.1 to 1. Note that when α is small (and hence ω_i is small), the e_i's are likely to be negative; when α is large, the e_i's are likely to be positive. From the figure, we clearly see that the robust methods outperform the non-robust methods. Moreover, we note that the robust methods perform better when the e_i's are more negative, which is consistent with our findings in Section IV-A.
- *Scenario 3*: In this scenario, we set $\omega_0 = 0.5$ and $\omega_i = 5\alpha$ for $i = 1, \ldots, 4$, where α varies from 0.1 to 1. In particular, the NLOS effect on the path from the source to the reference sensor is likely to be less pronounced than those from the source to the other sensors, which implies that the e_i's are likely to be positive. Our analysis in Section IV-A suggests that the robust methods may have a worse performance. This is confirmed by the results in Fig. 3. We also see that WLS-Non-Robust has the best performance when α is small.

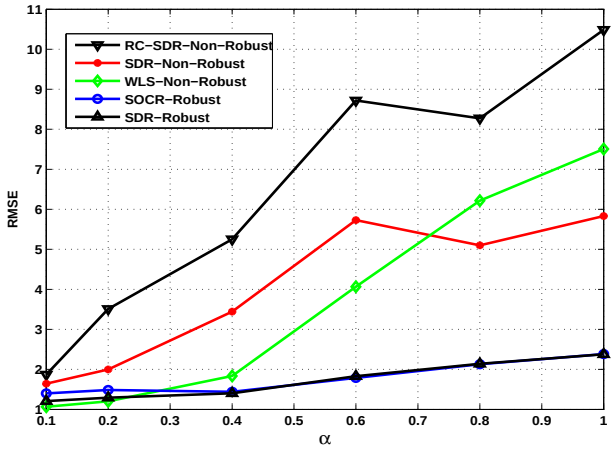

Fig. 1. Comparison of RMSE of different methods: $\sigma = 0.3$, $\omega_0 = 5\alpha$, and $\omega_i = 0.5$, where $i = 1, \ldots, 4$ and $\alpha = 0.1, 0.2, \ldots, 1$.

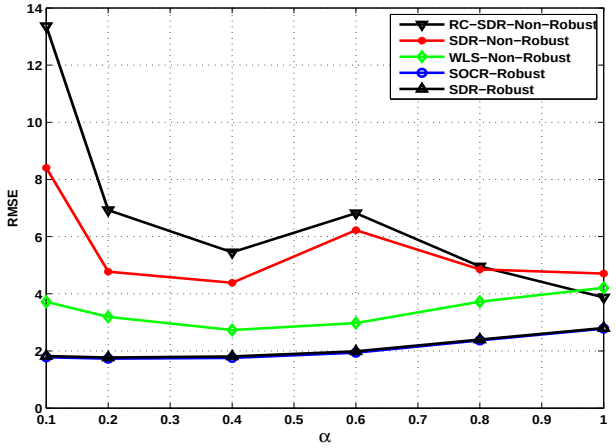

Fig. 2. Comparison of RMSE of different methods: $\sigma = 0.3$, $\omega_0 = 3$, and $\omega_i = 5\alpha$, where $i = 1, \ldots, 4$ and $\alpha = 0.1, 0.2, \ldots, 1$.

Summary: From Scenarios 1–3, we see that the performance of the robust methods is consistent with that predicted by the analysis in Section IV-A. In Table III, we record the number of MC runs in which SDR-Robust yields a solution $(\boldsymbol{Y}^*, \boldsymbol{y}^*, \boldsymbol{\tau}^*)$ that satisfies the rank condition $\text{rank}(\boldsymbol{Y}_{11}^*) \leq 1$ and hence uniquely localizes the source (see Proposition 5).[3] Out of all the instances tested, more than 93% of them can be uniquely localized by SDR-Robust, and that SDR-Robust tends to yield a unique localization of the source when the e_i's are more negative. It is also worth noting that when the e_i's are positive and have small magnitudes, WLS-Non-Robust has the best performance. However, its performance degrades rapidly as the e_i's become more negative. In comparison, the robust methods have rather stable performance in all investigated scenarios.

Group II: Varying the Power of Measurement Noise

[3]We regard $\boldsymbol{Y}_{11}^*$ to have rank at most one if the ratio between its second-largest and largest eigenvalue is less than 10^{-5}.

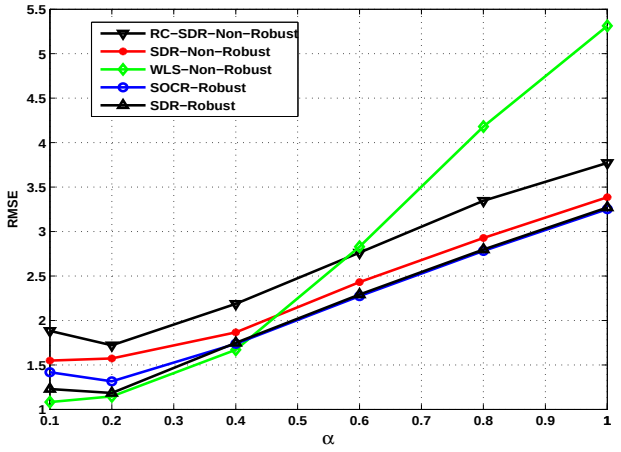

Fig. 3. Comparison of RMSE of different methods: $\sigma = 0.3$, $\omega_0 = 0.5$, and $\omega_i = 5\alpha$, where $i = 1, \ldots, 4$ and $\alpha = 0.1, 0.2, \ldots, 1$.

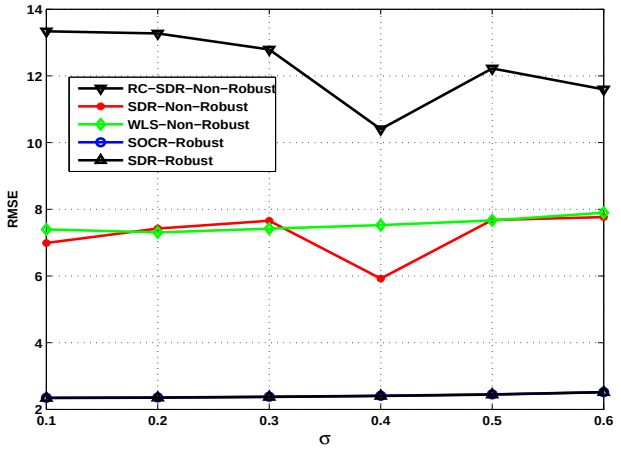

Fig. 4. Comparison of RMSE of different methods: $\sigma = 0.1, 0.2, \ldots, 0.6$, $\omega_0 = 5$, and $\omega_i = 0.5$ for $i = 1, \ldots, 4$.

TABLE III
NUMBER OF MC RUNS WITH RANK$(\boldsymbol{Y}_{11}^*) \leq 1$ FOR SCENARIOS 1–3
(3000 RUNS IN TOTAL)

α	0.1	0.2	0.4	0.6	0.8	1
Scenario 1	2623	2615	2871	2950	2989	2997
Scenario 2	2944	2912	2879	2787	2872	2867
Scenario 3	2619	2686	2773	2772	2763	2700

In this group of experiments, we fix the number of sensors at 5 (and hence $N = 4$). Moreover, in each of the scenarios below, we vary σ from 0.1 to 0.6.

- *Scenario 4*: In this scenario, we set $\omega_0 = 5$ and $\omega_i = 0.5$ for $i = 1, \ldots, 4$. Similar to Scenario 1, the e_i's are likely to be negative under this setting. Hence, based on the findings in Section IV-A, we expect the robust methods to perform well. As can be seen from Fig. 4, this is indeed the case. In fact, the robust methods perform significantly better than the non-robust methods. Moreover, the performance of the non-robust methods is not very stable, which suggests that these methods are sensitive to negative NLOS errors in the TDOA measurements.
- *Scenario 5*: In this scenario, we set $\omega_i = 3$ for $i = 0, 1, \ldots, 4$. Under this setting, the NLOS effect on all source-sensor paths are comparable. Hence, the e_i's can be small due to cancellations of the NLOS errors. Fig. 5 shows the performance of various methods. We see that the robust methods perform better than the non-robust methods. Also, WLS-Non-Robust performs better than SDR-Non-Robust. A possible explanation for this is that when the e_i's are small, SDR-Non-Robust can be fooled into thinking that the individual range measurements between the source and the sensors, which are introduced as decision variables in the formulation, also have small errors.
- *Scenario 6*: In this scenario, we set $\omega_0 = 0.5$ and $\omega_i = 5$ for $i = 1, \ldots, 4$. Similar to Scenario 3, the e_i's are likely to be positive under this setting. From Fig. 6, we see that the robust methods suffer some performance loss as compared to Scenario 4, which corroborates the analysis in Section IV-A.

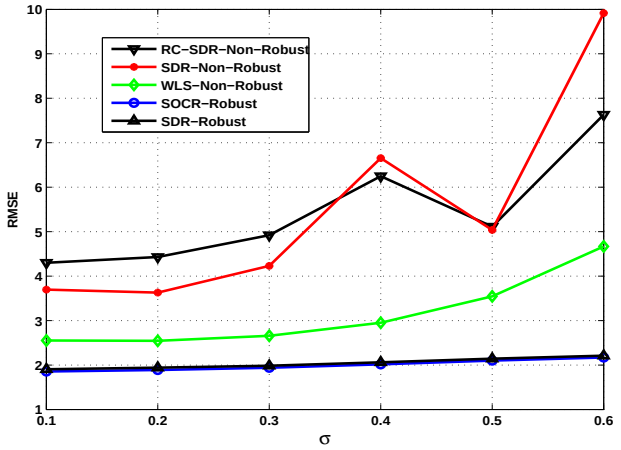

Fig. 5. Comparison of RMSE of different methods: $\sigma = 0.1, 0.2, \ldots, 0.6$ and $\omega_i = 3$ for $i = 0, 1, \ldots, 4$.

Summary: From Scenarios 4–6, we see that the performance of the robust methods is very stable, and the results support the findings in Section IV-A. SDR-Non-Robust and WLS-Non-Robust are not sensitive to positive e_i's. However, their performance becomes quite unstable and degrades dramatically in the presence of negative e_i's. A comparison of Fig. 4 and Fig. 6 reveals that positive e_i's cause a higher RMSE than negative ones, which is consistent with the analysis in [20]. Finally, in Table IV, we record the number of MC runs in which SDR-Robust uniquely localizes the source. Again, we see that a high percentage (more than 94%) of the tested instances can be uniquely localized by SDR-Robust, and that SDR-Robust tends to yield a unique localization of the source when the e_i's are more negative.

Group III: Varying the Number of Sensors

In this group of experiments, we set $\sigma = 0.3$. Moreover, in each of the scenarios below, we vary the number of sensors

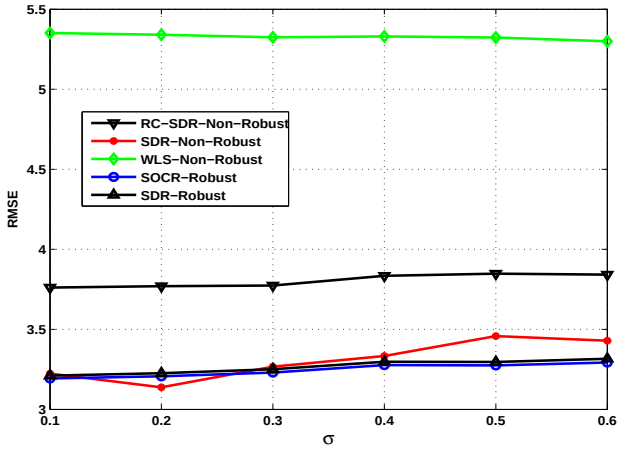

Fig. 6. Comparison of RMSE of different methods: $\sigma = 0.1, 0.2, \ldots, 0.6$, $\omega_0 = 0.5$, and $\omega_i = 5$ for $i = 1, \ldots, 4$.

TABLE IV
NUMBER OF MC RUNS WITH RANK$(\boldsymbol{Y}_{11}^*) \leq 1$ FOR SCENARIOS 4–6
(3000 RUNS IN TOTAL)

σ	0.1	0.2	0.3	0.4	0.5	0.6
Scenario 4	2999	2998	2997	2997	2992	2992
Scenario 5	2815	2844	2822	2821	2816	2794
Scenario 6	2681	2698	2709	2696	2690	2705

from 5 to 9 (and hence N varies from 4 to 8).

- *Scenario 7*: In this scenario, we set $\omega_0 = 5$ and $\omega_i = 0.5$ for $i = 1, \ldots, N$. Similar to Scenarios 1 and 4, the e_i's are likely to be negative under this setting. The performance of the various methods is shown in Fig. 7. As predicted by our analysis in Section IV-A, the robust methods perform quite well. On the other hand, we see that increasing the number of sensors generally improves the performance of the non-robust methods.

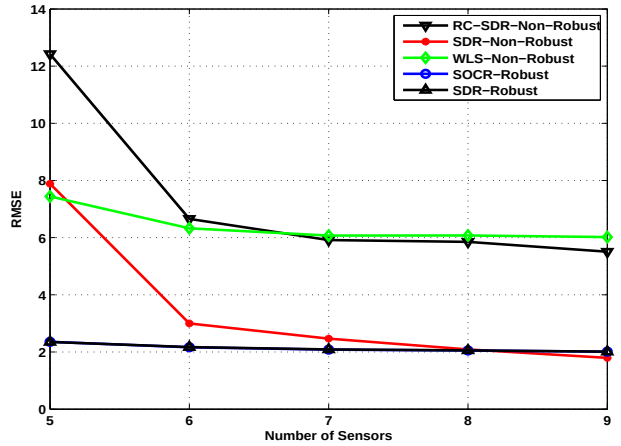

Fig. 7. Comparison of RMSE of different methods: $\sigma = 0.3$, $\omega_0 = 5$, and $\omega_i = 0.5$, where $i = 1, \ldots, N$ and $N = 4, 5, \ldots, 8$.

- *Scenario 8*: Fig. 8 shows the simulation results when $\sigma = 0.3$ and $\omega_i = 3$ for $i = 0, 1, \ldots, N$. Similar to Scenario 5, the e_i's can be small in this scenario. From the figure, we see that the performance of the robust methods dominates that of the non-robust methods. However, the non-robust methods do exhibit significant performance improvement as the number of sensors increases.

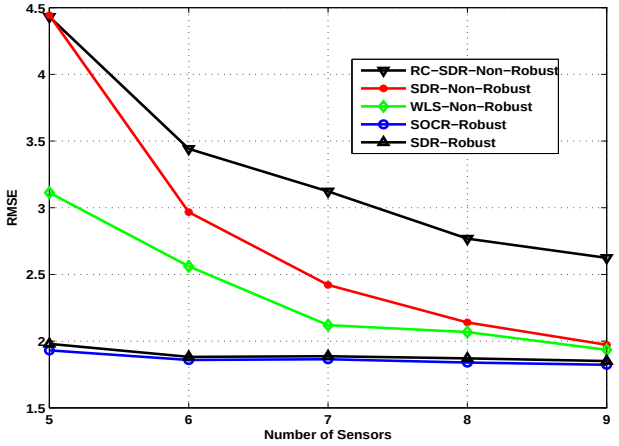

Fig. 8. Comparison of RMSE of different methods: $\sigma = 0.3$ and $\omega_i = 3$, where $i = 0, 1, \ldots, N$ and $N = 4, 5, \ldots, 8$.

- *Scenario 9*: In this scenario, we set $\omega_0 = 0.5$ and $\omega_i = 5$ for $i = 1, \ldots, N$. Similar to Scenarios 3 and 6, the e_i's are likely to be positive under this setting. The simulation results are shown in Fig. 9. As one would expect from the analysis in Section IV-A, the performance of the robust methods is rather marginal. In fact, SDR-Non-Robust performs better than the robust methods, and its performance improves as the number of sensors increases.

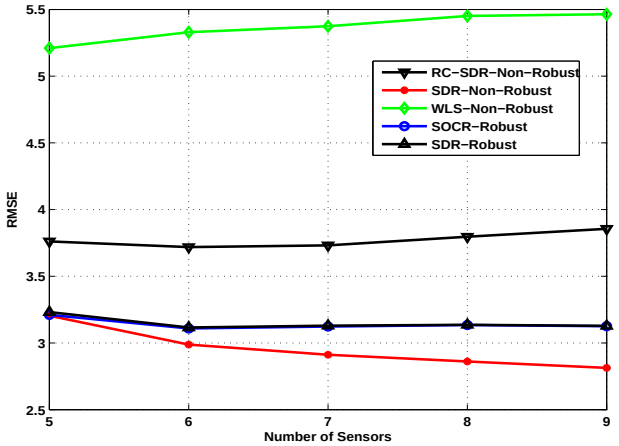

Fig. 9. Comparison of RMSE of different methods: $\sigma = 0.3$, $\omega_0 = 0.5$, and $\omega_i = 5$, where $i = 1, \ldots, N$ and $N = 4, 5, \ldots, 8$.

Summary: The results in Scenarios 7–9 show that while the performance of the non-robust methods improves as the number of sensors increases, the performance of the robust methods remains rather stable. This can be attributed to the conservatism of the robust methods. Indeed, the robust

methods are designed to guard against NLOS error vectors $\boldsymbol{e} = [e_1, \ldots, e_N]^T$ that lie inside the box $-\boldsymbol{\rho} \leq \boldsymbol{e} \leq \boldsymbol{\rho}$. However, in our experiments, we keep $\boldsymbol{\rho}$ fixed as the number of sensors increases. Thus, the robust methods are not exploiting the information offered by the additional sensors. Still, as can be seen from Fig. 7–Fig. 9, the performance of the robust methods is very competitive when compared to that of the non-robust methods. Finally, we record the number of MC runs in which SDR-Robust uniquely localizes the source in Table V. The results are in line with our earlier observations.

TABLE V
NUMBER OF MC RUNS WITH RANK$(\boldsymbol{Y}_{11}^*) \leq 1$ FOR SCENARIOS 7–9
(3000 RUNS IN TOTAL)

Number of Sensors	5	6	7	8	9
Scenario 7	2996	2998	2998	2998	2996
Scenario 8	2800	2882	2914	2926	2923
Scenario 9	2707	2670	2649	2668	2651

2) Sensitivity to Inaccurate Upper Bounds: We now turn to investigate the performance sensitivity of the proposed robust methods to the upper bounds on e_i's magnitudes. Suppose that instead of the nominal upper bound on $|e_i|$, namely ρ_i, we use an inaccurate upper bound of the form $\tilde{\rho}_i = \rho_i(1+\delta)$, where δ is uniformly distributed between $-\beta$ and β. The performance sensitivity is measured by the relative change in RMSE; i.e.,

$$\gamma = \frac{\text{RMSE}(\tilde{\boldsymbol{\rho}}) - \text{RMSE}(\boldsymbol{\rho})}{\text{RMSE}(\boldsymbol{\rho})} \times 100\%,$$

where $\boldsymbol{\rho} = [\rho_1, \ldots, \rho_N]^T$ and $\tilde{\boldsymbol{\rho}} = [\tilde{\rho}_1, \ldots, \tilde{\rho}_N]^T$, and RMSE$(\boldsymbol{\rho})$ and RMSE$(\tilde{\boldsymbol{\rho}})$ are the RMSE when the nominal and inaccurate upper bounds are used, respectively. We fix the number of sensors at 5 (and hence $N = 4$) and vary β from 0.05 to 0.3. The performance of the robust methods under different levels of NLOS errors in the TDOA measurements is shown in Fig. 10–Fig. 12. From the figures, we see that the robust methods are relatively insensitive to inaccuracies in the upper bounds, and the RMSE has a notable increase only when $\beta = 0.3$.

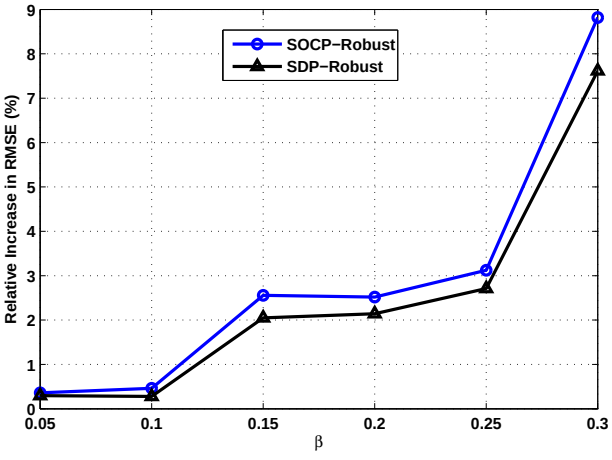

Fig. 10. Sensitivity of the robust methods to inaccurate upper bounds: $\beta = 0.05, 0.1, \ldots, 0.3$, $\sigma = 0.3$, $\omega_0 = 0.5$, and $\omega_i = 5$ for $i = 1, \ldots, 4$.

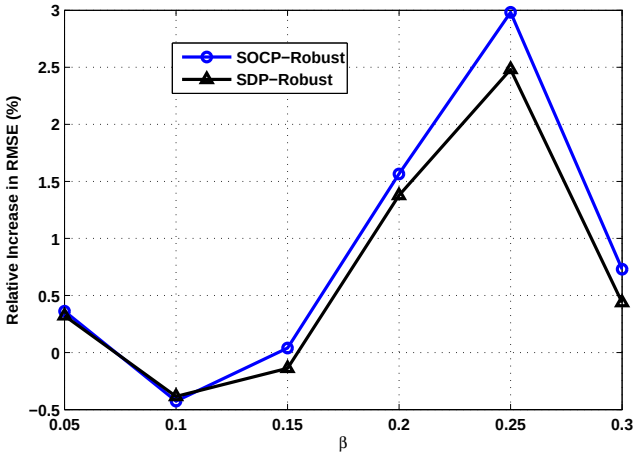

Fig. 11. Sensitivity of the robust methods to inaccurate upper bounds: $\beta = 0.05, 0.1, \ldots, 0.3$, $\sigma = 0.3$, and $\omega_i = 3$ for $i = 0, 1, \ldots, 4$.

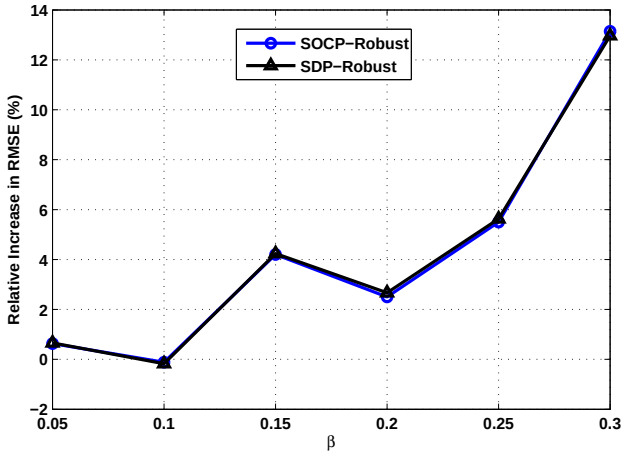

Fig. 12. Sensitivity of the robust methods to inaccurate upper bounds: $\beta = 0.05, 0.1, \ldots, 0.3$, $\sigma = 0.3$, $\omega_0 = 5$, and $\omega_i = 0.5$ for $i = 1, \ldots, 4$.

B. Performance Evaluation Using Real Data

In this subsection, we test the various methods using real measurement data downloaded from [40]. The detailed description of the dataset can be found in [41]; here we summarize its key aspects. There are 44 nodes deployed in a room of area 14m $\times$ 13m, whose locations are shown in Fig. 13 (nodes that are used as sensors are marked by a triangle ($\triangle$); see more details below). Each node can communicate with any other node, and the NLOS TOA measurement between node i and node j (for $i, j \in \{1, \ldots, 44\}$ and $i \neq j$) is modeled as

$$\tilde{T}_{ij} = \frac{1}{c}\|\boldsymbol{s}_i - \boldsymbol{s}_j\| + \mu_{\text{TOA}} + \frac{1}{c}\left(\tilde{n}_{ij} + \tilde{e}_{ij}\right), \qquad (23)$$

where $\boldsymbol{s}_i$ and $\boldsymbol{s}_j$ are the locations of node i and node j, respectively; μ_{TOA} is the mean positive bias of the TOA measurement due to NLOS propagation of signals; $\frac{1}{c}\tilde{n}_{ij}$ and $\mu_{\text{TOA}} + \frac{1}{c}\tilde{e}_{ij}$ are the measurement noise and NLOS error in the TOA measurement, respectively. The aggregate TOA measurement error $\tilde{\varepsilon}_{ij} = \tilde{n}_{ij} + \tilde{e}_{ij}$ is assumed to have

mean zero and standard deviation $c\sigma_{\text{TOA}}$. Moreover, the errors $\{\tilde{\varepsilon}_{ij}\}_{i,j}$ are assumed to be independent. Although the precise values of μ_{TOA} and σ_{TOA} are not known, they can be estimated from the measurement data. Specifically, the sample estimates of μ_{TOA} and σ_{TOA} are $\hat{\mu}_{\text{TOA}} = 10.9\text{ns}$ and $\hat{\sigma}_{\text{TOA}} = 6.1\text{ns}$, respectively. The estimated TOA measurement bias $\hat{\mu}_{\text{TOA}}$ is then subtracted from the NLOS TOA measurements to form unbiased (or LOS) TOA measurements. In other words, the LOS TOA measurement between node i and node j (for $i, j \in \{1, \ldots, 44\}$ and $i \neq j$) is given by $\bar{T}_{ij} = \tilde{T}_{ij} - \hat{\mu}_{\text{TOA}}$.

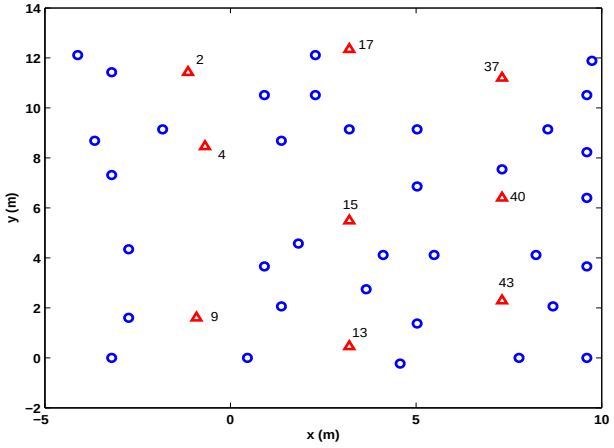

Fig. 13. Sensor and source geometry in a real room [41]: △: sensor, ○: source.

For our experiments, we need to extract NLOS TDOA measurements from the LOS TOA measurements in the dataset. This is done using (23). Specifically, given a node $k \in \{1, \ldots, 44\}$, we obtain the NLOS TDOA measurement T_{ij}^k between node i and node j with respect to node k (for $i, j \in \{1, \ldots, 44\}$, $i > j$, $k \neq i$, and $k \neq j$) by

$$T_{ij}^k = \tilde{T}_{ik} - \tilde{T}_{jk} = \bar{T}_{ik} - \bar{T}_{jk}. \tag{24}$$

Upon expanding (24), we have

$$\begin{aligned} T_{ij}^k &= \frac{1}{c}(\|\boldsymbol{s}_i - \boldsymbol{s}_k\| - \|\boldsymbol{s}_j - \boldsymbol{s}_k\|) + \frac{1}{c}\left(\tilde{n}_{ik} - \tilde{n}_{jk} + \tilde{e}_{ik} - \tilde{e}_{jk}\right) \\ &= \frac{1}{c}(\|\boldsymbol{s}_i - \boldsymbol{s}_k\| - \|\boldsymbol{s}_j - \boldsymbol{s}_k\|) + \frac{1}{c}\left(n_{ij}^k + e_{ij}^k\right), \end{aligned}$$

where $n_{ij}^k = \tilde{n}_{ik} - \tilde{n}_{jk}$ and $e_{ij}^k = \tilde{e}_{ik} - \tilde{e}_{jk}$ are the measurement noise and NLOS error in the TDOA measurement, respectively. Using the statistics of $\{\tilde{\varepsilon}_{ij}\}_{i,j}$, it can be deduced that the aggregate TDOA measurement error $\varepsilon_{ij}^k = n_{ij}^k + e_{ij}^k = \tilde{\varepsilon}_{ik} - \tilde{\varepsilon}_{jk}$ has mean zero and standard deviation $\sqrt{2}c\sigma_{\text{TOA}}$. To gain further insights into the distribution of ε_{ij}^k, we plot both the histogram of the values $\left\{\varepsilon_{ij}^k\right\}_{i,j,k}$ obtained from the dataset and the probability density function (PDF) of the Gaussian distribution $\mathcal{N}\left(0, 2c^2\hat{\sigma}_{\text{TOA}}^2\right)$ in Fig. 14. As can be seen from the figure, the empirical distribution of the values $\left\{\varepsilon_{ij}^k\right\}_{i,j,k}$ is well approximated by the Gaussian distribution. Hence, we shall assume that ε_{ij}^k follows the Gaussian distribution $\mathcal{N}\left(0, 2c^2\hat{\sigma}_{\text{TOA}}^2\right)$.

To test our proposed robust methods, we also need to derive an upper bound on the magnitudes of the NLOS errors in the TDOA measurements. Towards that end, we first note that the magnitudes of the TDOA measurement noise are typically much smaller than the largest magnitude of the NLOS errors. In other words, we may assume that $\left|n_{ij}^k\right| \ll \max_{i,j,k}\left|e_{ij}^k\right|$ for $i, j, k \in \{1, \ldots, 44\}$ with $i > j$, $k \neq i$, and $k \neq j$. Consequently, the largest magnitude of the NLOS errors can be approximated by that of the aggregate TDOA measurement errors; i.e.,

$$\max_{i,j,k}\left|e_{ij}^k\right| \approx \max_{i,j,k}\left|n_{ij}^k + e_{ij}^k\right| = \max_{i,j,k}\left|\varepsilon_{ij}^k\right|.$$

Now, since ε_{ij}^k is assumed to follow the distribution $\mathcal{N}\left(0, 2c^2\hat{\sigma}_{\text{TOA}}^2\right)$, with a probability of 99%, it will satisfy $\left|\varepsilon_{ij}^k\right| \leq 2.58\sqrt{2}c\hat{\sigma}_{\text{TOA}} = 6.6724\text{m}$. Thus, for practical purposes, we may use $\rho = 6.6724$ as an upper bound on the magnitudes of the NLOS errors in the TDOA measurements.

Similar to Scenarios 7–9, we vary the number of sensors from 5 to 9 (and hence N varies from 4 to 8) and study the impact on the localization performance of various methods. For $N = 8$, the set of indices of nodes that are chosen as sensors is $\mathcal{I} = \{15, 2, 9, 43, 37, 13, 17, 4, 40\}$ (the chosen nodes are marked by "△" in Fig. 13); for $N = 4, 5, 6$ or 7, the nodes corresponding to the first N indices in $\mathcal{I}$ are chosen as sensors. The index set $\mathcal{I}$ is constructed by first choosing 5 sensors with one sensor (node 15) at the center and the other four (nodes 2, 9, 43, and 37) lying approximately on a circle, and then adding sensors that are lying approximately on the circle until a total of 9 sensors is reached. After fixing the $N + 1$ sensors, the remaining $44 - (N + 1)$ nodes are regarded as different sources. For each source, we construct the NLOS TDOA measurements according to (24) with node 15 as the reference sensor. Finally, the localization performance is measured by the RMSE criterion (22), with $M = 44-(N+1)$. This completes the description of our experimental setup.

Fig. 15 shows the localization performance of the different methods. We see that our proposed methods have the best performance when the number of sensors is small. On the other hand, the performance of SDR-Non-Robust improves as

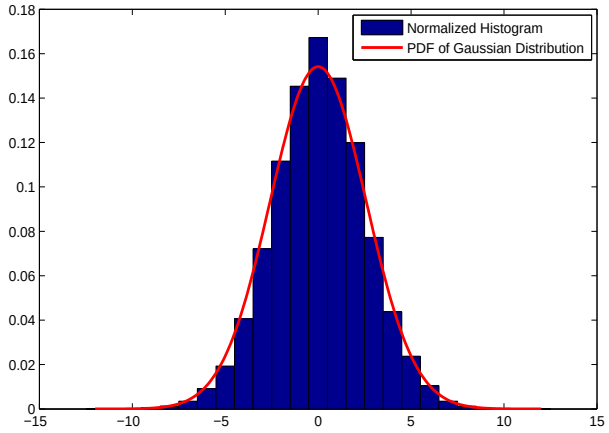

Fig. 14. Comparison of the histogram of the values $\left\{\varepsilon_{ij}^k\right\}_{i,j,k}$ and the PDF of $\mathcal{N}\left(0, 2c^2\hat{\sigma}_{\text{TOA}}^2\right)$.

the number of sensors increases. The results are in line with those obtained using synthetic data.

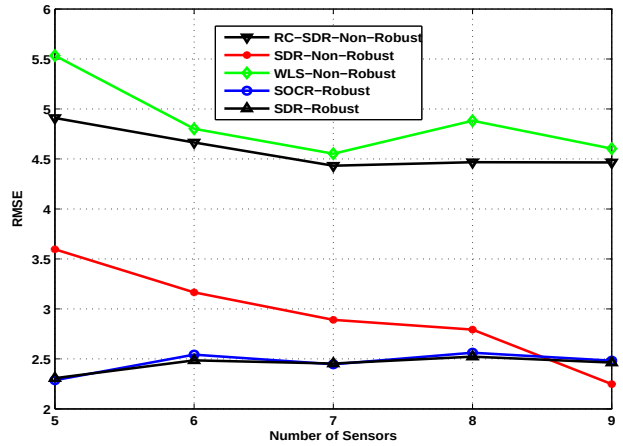

Fig. 15. Comparison of RMSE of different methods using real data: $\rho = 6.6724$ and $N = 4, 5, \ldots, 8$.

Next, we compare the average running times of the various methods in Fig. 16. From the figure, we see that SOCR-Robust takes less computation time than SDR-Robust, which corroborates the analysis in Section IV-C. We also see that WLS-Non-Robust and SDR-Non-Robust take the least and most computation time, respectively. It should be noted that the comparison may not be fair, as WLS-Non-Robust is implemented using problem-specific codes, while the other four methods are implemented using a universal solver.

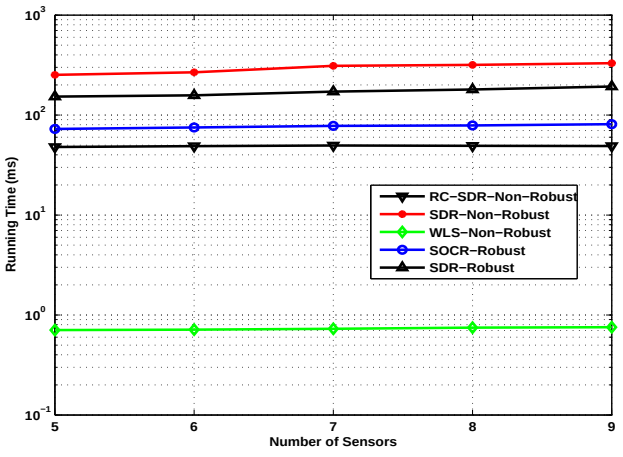

Fig. 16. Comparison of average running times of different methods using real data: $\rho = 6.6724$ and $N = 4, 5, \ldots, 8$.

VI. Conclusion

In this paper, we presented an RLS formulation of the TDOA-based source localization problem under NLOS conditions. To tackle the non-convexity of the RLS problem, we developed a two-step approach, where we first construct an auxiliary problem to approximate the RLS problem and then apply convex relaxation techniques to the former to obtain two efficiently solvable convex approximations. Next, we analyzed the quality and complexity of the proposed approximations. In particular, we identified the conditions under which the auxiliary problem is equivalent to the RLS problem and established sufficient conditions under which the two convex approximations will yield a unique localization of the source. Extensive simulations on both synthetic and real data showed that the proposed methods are robust against both NLOS errors and inaccurate upper bounds on the magnitudes of the NLOS errors. Moreover, the simulation results corroborated the findings in our theoretical analysis. An interesting open question is to determine whether the sufficient condition stated in Proposition 5 is also necessary for the refined SDR (21) to yield a unique localization of the source. We conjecture that the answer is affirmative.

Appendix
Proof of Proposition 2

Observe that

$$\begin{aligned}&\left|\boldsymbol{a}_i^T\boldsymbol{y} - b_i + e_i^2 - 2(d_i - r_i)e_i\right| \\ &= \left|(e_i - (d_i - r_i))^2 + \left(\boldsymbol{a}_i^T\boldsymbol{y} - b_i\right) - (d_i - r_i)^2\right|.\end{aligned}$$

Thus, if $|d_i - r_i| \le \rho_i$, then

$$\begin{aligned}&\max_{-\rho_i \le e_i \le \rho_i} \left|\boldsymbol{a}_i^T\boldsymbol{y} - b_i + e_i^2 - 2(d_i - r_i)e_i\right| \\ &= \max\Big\{\left|(\pm\rho_i - (d_i - r_i))^2 + \left(\boldsymbol{a}_i^T\boldsymbol{y} - b_i\right) - (d_i - r_i)^2\right|, \\ &\qquad \left|\boldsymbol{a}_i^T\boldsymbol{y} - b_i - (d_i - r_i)^2\right|\Big\} \\ &= \max\Big\{\left|\boldsymbol{a}_i^T\boldsymbol{y} - b_i \pm 2\rho_i(d_i - r_i) + \rho_i^2\right|, \\ &\qquad \left|\boldsymbol{a}_i^T\boldsymbol{y} - b_i - (d_i - r_i)^2\right|\Big\}.\end{aligned}$$

On the other hand, if $|d_i - r_i| > \rho_i$, then

$$\begin{aligned}&\max_{-\rho_i \le e_i \le \rho_i} \left|\boldsymbol{a}_i^T\boldsymbol{y} - b_i + e_i^2 - 2(d_i - r_i)e_i\right| \\ &= \max\left\{\left|\boldsymbol{a}_i^T\boldsymbol{y} - b_i \pm 2\rho_i(d_i - r_i) + \rho_i^2\right|\right\}.\end{aligned}$$

Hence, we have

$$\begin{aligned}&\max_{-\rho_i \le e_i \le \rho_i} \left|\boldsymbol{a}_i^T\boldsymbol{y} - b_i + e_i^2 - 2(d_i - r_i)e_i\right| \\ &= \begin{cases} \max\left\{|u_i^+|, |u_i^-|, |v_i|\right\} & \text{if } |d_i - r_i| \le \rho_i, \\ \max\left\{|u_i^+|, |u_i^-|\right\} & \text{otherwise,} \end{cases}\end{aligned} \tag{25}$$

where

$$\begin{aligned} u_i^+ &= \boldsymbol{a}_i^T\boldsymbol{y} - b_i + 2\rho_i(d_i - r_i) + \rho_i^2, \\ u_i^- &= \boldsymbol{a}_i^T\boldsymbol{y} - b_i - 2\rho_i(d_i - r_i) + \rho_i^2, \\ v_i &= \boldsymbol{a}_i^T\boldsymbol{y} - b_i - (d_i - r_i)^2. \end{aligned}$$

To establish the desired result, consider the following three cases:

Case 1: $\boldsymbol{a}_i^T\boldsymbol{y} - b_i \ge 0$.

We have

$$\begin{aligned}&\max_{-\rho_i \le e_i \le \rho_i} \left|\boldsymbol{a}_i^T\boldsymbol{y} - b_i + e_i^2 - 2(d_i - r_i)e_i\right| \\ &= \boldsymbol{a}_i^T\boldsymbol{y} - b_i + \max_{-\rho_i \le e_i \le \rho_i} \left|e_i^2 - 2(d_i - r_i)e_i\right| \\ &= \boldsymbol{a}_i^T\boldsymbol{y} - b_i + 2\rho_i|d_i - r_i| + \rho_i^2.\end{aligned}$$

Case 2: $\boldsymbol{a}_i^T\boldsymbol{y} - b_i < 0$ and $|d_i - r_i| \leq \rho_i$.

Since $\boldsymbol{a}_i^T\boldsymbol{y} - b_i < 0$, we have $|v_i| = (d_i - r_i)^2 - \big(\boldsymbol{a}_i^T\boldsymbol{y} - b_i\big)$. This implies that $|v_i| + u_i^+ = (d_i - r_i + \rho_i)^2 \geq 0$ and $|v_i| + u_i^- = (d_i - r_i - \rho_i)^2 \geq 0$. Consider further the following sub-cases:

Case 2a: $d_i - r_i \geq 0$ and $u_i^+ < 0$.

Then, we have $u_i^- \leq u_i^+ < 0$, which implies that $|v_i| \geq -u_i^- = \max\big\{|u_i^+|, |u_i^-|\big\}$.

Case 2b: $d_i - r_i \geq 0$ and $u_i^+ \geq 0$.

If $u_i^- \geq 0$, then $|u_i^+| = u_i^+ \geq u_i^- = |u_i^-|$. Otherwise, we have $|v_i| \geq -u_i^- = |u_i^-|$. It follows that $\max\big\{|u_i^+|, |v_i|\big\} \geq |u_i^-|$.

Case 2c: $d_i - r_i < 0$ and $u_i^- < 0$.

Then, we have $u_i^+ \leq u_i^- < 0$, which implies that $|v_i| \geq -u_i^+ = \max\big\{|u_i^+|, |u_i^-|\big\}$.

Case 2d: $d_i - r_i < 0$ and $u_i^- \geq 0$.

If $u_i^+ \geq 0$, then $|u_i^-| = u_i^- \geq u_i^+ = |u_i^+|$. Otherwise, we have $|v_i| \geq -u_i^+ = |u_i^+|$. It follows that $\max\big\{|u_i^-|, |v_i|\big\} \geq |u_i^+|$.

Upon combining the above sub-cases, we conclude that

$$\begin{aligned}
&\max\big\{|u_i^+|, |u_i^-|, |v_i|\big\} \\
&= \max\big\{\boldsymbol{a}_i^T\boldsymbol{y} - b_i + 2\rho_i|d_i - r_i| + \rho_i^2, \\
&\qquad\qquad (d_i - r_i)^2 - \big(\boldsymbol{a}_i^T\boldsymbol{y} - b_i\big)\big\}.
\end{aligned}$$

Case 3: $\boldsymbol{a}_i^T\boldsymbol{y} - b_i < 0$ and $|d_i - r_i| > \rho_i$.

It follows directly from (25) that

$$\begin{aligned}
&\max_{-\rho_i \leq e_i \leq \rho_i} \big|\boldsymbol{a}_i^T\boldsymbol{y} - b_i + e_i^2 - 2(d_i - r_i)e_i\big| \\
&= \max\big\{\big|\boldsymbol{a}_i^T\boldsymbol{y} - b_i \pm 2\rho_i(d_i - r_i) + \rho_i^2\big|\big\}.
\end{aligned}$$

REFERENCES

[1] D. N. Hatfield, "A report on technical and operational issues impacting the provision of wireless enhanced 911 services," Federal Communications Commission and Department of Transportation, Washington, DC, Tech. Rep., 2003.

[2] K. Lorincz, D. J. Malan, T. R. F. Fulford-Jones, A. Nawoj, A. Clavel, V. Shnayder, G. Mainland, M. Welsh, and S. Moulton, "Sensor networks for emergency response: Challenges and opportunities," *IEEE Pervasive Computing*, vol. 3, no. 4, pp. 16–23, 2004.

[3] S. J. Vaughan-Nichols, "Will mobile computing's future be location, location, location?" *Computer*, vol. 42, no. 2, pp. 14–17, 2009.

[4] K. Zhou and S. I. Roumeliotis, "Multirobot active target tracking with combinations of relative observations," *IEEE Transactions on Robotics*, vol. 27, no. 4, pp. 678–695, 2011.

[5] N. Patwari, J. N. Ash, S. Kyperountas, A. O. Hero III, R. L. Moses, and N. S. Correal, "Locating the nodes: Cooperative localization in wireless sensor networks," *IEEE Signal Processing Magazine*, vol. 22, no. 4, pp. 54–69, 2005.

[6] A. H. Sayed, A. Tarighat, and N. Khajehnouri, "Network–based wireless location: Challenges faced in developing techniques for accurate wireless location information," *IEEE Signal Processing Magazine*, vol. 22, no. 4, pp. 24–40, 2005.

[7] I. Güvenç and C.-C. Chong, "A survey on TOA based wireless localization and NLOS mitigation techniques," *IEEE Communications Surveys and Tutorials*, vol. 11, no. 3, pp. 107–124, 2009.

[8] J. Khodjaev, Y. Park, and A. S. Malik, "Survey on NLOS identification and error mitigation problems in UWB–based positioning algorithms for dense environments," *Annals of Telecommunications*, vol. 65, no. 5–6, pp. 301–311, 2010.

[9] A. Prorok, L. Gonon, and A. Martinoli, "Online model estimation of ultra–wideband TDOA measurements for mobile robot localization," in *Proceedings of the 2012 IEEE International Conference on Robotics and Automation (ICRA 2012)*, 2012, pp. 807–814.

[10] H. Wymeersch, S. Maranò, W. M. Gifford, and M. Z. Win, "A machine learning approach to ranging error mitigation for UWB localization," *IEEE Transactions on Communications*, vol. 60, no. 6, pp. 1719–1728, 2012.

[11] F. Yin, C. Fritsche, F. Gustafsson, and A. M. Zoubir, "EM– and JMAP–ML based joint estimation algorithms for robust wireless geolocation in mixed LOS/NLOS environments," *IEEE Transactions on Signal Processing*, vol. 62, no. 1, pp. 168–182, 2014.

[12] S. Nawaz and N. Trigoni, "Convex programming based robust localization in NLOS prone cluttered environments," in *Proceedings of the 10th International Conference on Information Processing in Sensor Networks (IPSN 2011)*, 2011, pp. 318–329.

[13] R. M. Vaghefi, J. Schloemann, and R. M. Buehrer, "NLOS mitigation in TOA–based localization using semidefinite programming," in *Proceedings of the 10th IEEE Workshop on Positioning, Navigation and Communication (WPNC 2013)*, 2013, pp. 1–6.

[14] G. Wang, H. Chen, Y. Li, and N. Ansari, "NLOS error mitigation for TOA–based localization via convex relaxation," *IEEE Transactions on Wireless Communications*, vol. 13, no. 8, pp. 4119–4131, 2014.

[15] C.-H. Park, S. Lee, and J.-H. Chang, "Robust closed–form time–of–arrival source localization based on α–trimmed mean and Hodges–Lehmann estimator under NLOS environments," *Signal Processing*, vol. 111, pp. 113–123, 2015.

[16] L. Cong and W. Zhuang, "Nonline–of–sight error mitigation in mobile location," *IEEE Transactions on Wireless Communications*, vol. 4, no. 2, pp. 560–573, 2005.

[17] S. Venkatesh and R. M. Buehrer, "NLOS mitigation using linear programming in ultrawideband location–aware networks," *IEEE Transactions on Vehicular Technology*, vol. 56, no. 5, pp. 3182–3198, 2007.

[18] K. Yang, J. An, X. Bu, and Y. Lu, "A TOA–based location algorithm for NLOS environments using quadratic programming," in *Proceedings of the 2010 IEEE Wireless Communications and Networking Conference (WCNC 2010)*, 2010.

[19] H. Chen, G. Wang, Z. Wang, H. C. So, and H. V. Poor, "Non–line–of–sight node localization based on semi–definite programming in wireless sensor networks," *IEEE Transactions on Wireless Communications*, vol. 11, no. 1, pp. 108–116, 2012.

[20] S. Hara, D. Anzai, T. Yabu, K. Lee, T. Derham, and R. Zemek, "A perturbation analysis on the performance of TOA and TDOA localization in mixed LOS/NLOS environments," *IEEE Transactions on Communications*, vol. 61, no. 2, pp. 679–689, 2013.

[21] A. Ben-Tal and A. Nemirovski, *Lectures on Modern Convex Optimization: Analysis, Algorithms, and Engineering Applications*, ser. MPS–SIAM Series on Optimization. Philadelphia, Pennsylvania: Society for Industrial and Applied Mathematics, 2001.

[22] M. Grant and S. Boyd, "CVX: Matlab software for disciplined convex programming, version 2.1," http://cvxr.com/cvx, 2014.

[23] A. M.-C. So and Y. Ye, "Theory of semidefinite programming for sensor network localization," *Mathematical Programming, Series B*, vol. 109, no. 2, pp. 367–384, 2007.

[24] P. Tseng, "Second–order cone programming relaxation of sensor network localization," *SIAM Journal on Optimization*, vol. 18, no. 1, pp. 156–185, 2007.

[25] G. Naddafzadeh-Shirazi, M. B. Shenouda, and L. Lampe, "Second order cone programming for sensor network localization with anchor position uncertainty," *IEEE Transactions on Wireless Communications*, vol. 13, no. 2, pp. 749–763, 2014.

[26] U. Hammes, E. Wolsztynski, and A. M. Zoubir, "Robust tracking and geolocation for wireless networks in NLOS environments," *IEEE Journal of Selected Topics in Signal Processing*, vol. 3, no. 5, pp. 889–901, 2009.

[27] K. Yang, G. Wang, and Z.-Q. Luo, "Efficient convex relaxation methods for robust target localization by a sensor network using time difference of arrivals," *IEEE Transactions on Signal Processing*, vol. 57, no. 7, pp. 2775–2784, 2009.

[28] Y. T. Chan and K. C. Ho, "A simple and efficient estimator for hyperbolic location," *IEEE Transactions on Signal Processing*, vol. 42, no. 8, pp. 1905–1915, 1994.

[29] R. Exel, G. Gaderer, and P. Loschmidt, "Localisation of wireless LAN nodes using accurate TDoA measurements," in *Proceedings of the 2010 IEEE Wireless Communications and Networking Conference (WCNC 2010)*, 2010.

[30] B. Schölkopf, J. C. Platt, J. Shawe-Taylor, A. J. Smola, and R. C. Williamson, "Estimating the support of a high–dimensional distribution," *Neural Computation*, vol. 13, no. 7, pp. 1443–1471, 2001.

[31] Z.-Q. Luo, W.-K. Ma, A. M.-C. So, Y. Ye, and S. Zhang, "Semidefinite relaxation of quadratic optimization problems," *IEEE Signal Processing Magazine*, vol. 27, no. 3, pp. 20–34, 2010.
[32] K.-Y. Wang, A. M.-C. So, T.-H. Chang, W.-K. Ma, and C.-Y. Chi, "Outage constrained robust transmit optimization for multiuser MISO downlinks: Tractable approximations by conic optimization," *IEEE Transactions on Signal Processing*, vol. 62, no. 21, pp. 5690–5705, 2014.
[33] E. de Klerk, C. Roos, and T. Terlaky, "Initialization in semidefinite programming via a self–dual skew–symmetric embedding," *Operations Research Letters*, vol. 20, pp. 213–221, 1997.
[34] K. W. K. Lui, F. K. W. Chan, and H. C. So, "Semidefinite programming approach for range–difference based source localization," *IEEE Transactions on Signal Processing*, vol. 57, no. 4, pp. 1630–1633, 2009.
[35] K. W. Cheung, H. C. So, W.-K. Ma, and Y. T. Chan, "A constrained least squares approach to mobile positioning: Algorithms and optimality," *EURASIP Journal on Applied Signal Processing*, vol. 2006, no. 20858, pp. 1–23, 2006.
[36] A. Beck, P. Stoica, and J. Li, "Exact and approximate solutions of source localization problems," *IEEE Transactions on Signal Processing*, vol. 56, no. 5, pp. 1770–1778, 2008.
[37] L. Lin, H. C. So, F. K. W. Chan, Y. T. Chan, and K. C. Ho, "A new constrained weighted least squares algorithm for TDOA–based localization," *Signal Processing*, vol. 93, no. 11, pp. 2872–2878, 2013.
[38] E. Xu, Z. Ding, and S. Dasgupta, "Reduced complexity semidefinite relaxation algorithms for source localization based on time difference of arrival," *IEEE Transactions on Mobile Computing*, vol. 10, no. 9, pp. 1276–1282, 2011.
[39] K.-C. Toh, M. J. Todd, and R. H. Tütüncü, "On the implementation and usage of SDPT3 – a MATLAB software package for semidefinite–quadratic–linear programming, version 4.0," in *Handbook on Semidefinite, Conic and Polynomial Optimization*, ser. International Series in Operations Research and Management Science, M. F. Anjos and J. B. Lasserre, Eds. New York: Springer Science+Business Media, LLC, 2012, vol. 166, pp. 715–754.
[40] N. Patwari, "Wireless sensor network localization measurement repository," http://www.eecs.umich.edu/~hero/localize, 2006.
[41] N. Patwari, A. O. Hero, M. Perkins, N. S. Correal, and R. J. O'Dea, "Relative location estimation in wireless sensor networks," *IEEE Transactions on Signal Processing*, vol. 51, no. 8, pp. 2137–2148, 2003.

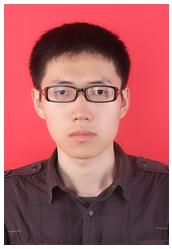

Gang Wang (M'13) received the B.Eng. degree from Shandong University, Jinan, China, and the Ph.D. degree from Xidian University, Xi'an, China, both in electrical engineering, in 2006 and 2011, respectively. He joined Ningbo University, Ningbo, China, in January 2012, and he is currently an Associate Professor. His research interests are in the area of target localization and tracking in wireless networks.

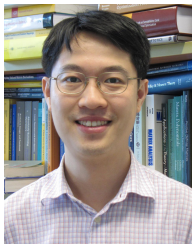

Anthony Man-Cho So (M'12) received his BSE degree in Computer Science from Princeton University with minors in Applied and Computational Mathematics, Engineering and Management Systems, and German Language and Culture. He then received his MSc degree in Computer Science and his PhD degree in Computer Science with a PhD minor in Mathematics from Stanford University. Dr. So joined The Chinese University of Hong Kong (CUHK) in 2007. He currently serves as Assistant Dean of the Faculty of Engineering and is an Associate Professor in the Department of Systems Engineering and Engineering Management. He also holds a courtesy appointment as Associate Professor in the CUHK-BGI Innovation Institute of Trans-omics. His recent research focuses on the interplay between optimization theory and various areas of algorithm design, such as computational geometry, machine learning, signal processing, bioinformatics, and algorithmic game theory.

Dr. So currently serves on the editorial boards of IEEE TRANSACTIONS ON SIGNAL PROCESSING, Journal of Global Optimization, Optimization Methods and Software, and SIAM Journal on Optimization. He has also served on the editorial board of Mathematics of Operations Research. He received the 2015 IEEE Signal Processing Society Signal Processing Magazine Best Paper Award, the 2014 IEEE Communications Society Asia-Pacific Outstanding Paper Award, the 2010 Institute for Operations Research and the Management Sciences (INFORMS) Optimization Society Optimization Prize for Young Researchers, and the 2010 CUHK Young Researcher Award. He also received the 2008 Exemplary Teaching Award and the 2011, 2013, 2015 Dean's Exemplary Teaching Award from the Faculty of Engineering at CUHK, and the 2013 Vice-Chancellor's Exemplary Teaching Award from CUHK.

Youming Li received the B.S. degree in computational mathematics from Lanzhou University, China, in 1985, the M.S. degree in computational mathematics from Xi'an Jiaotong University, Xi'an, China, in 1988, and the Ph.D. degree in electrical Engineering from Xidian University, Xi'an, China, in 1995. From 1988 to 1998, he worked in the Department of Applied Mathematics, Xidian University, where he was an Associate Professor. From 1999 to 2004, he worked in the School of Electrical and Electronics Engineering, Nanyang Technological University, DSO National Laboratories, Singapore, and the School of Engineering, Bar-Ilan University, Israel, respectively. Since 2005, he has been with Ningbo University, Ningbo, China, where he is currently a Professor. His research interests are in cognitive radio and wireless/wireline communications.